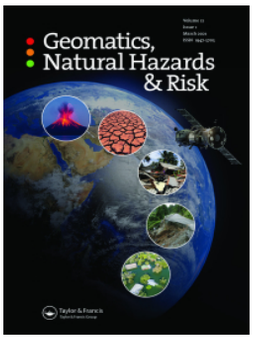

Geomatics, Natural Hazards and Risk

ISSN: 1947-5705 (Print) 1947-5713 (Online) Journal homepage: www.tandfonline.com/journals/tgnh20

Comprehensive hazard susceptibility assessment in Port Sudan city using AHP: emphasizing flash flood risk, soil moisture, and salinity dynamics

Abazar M. A. Daoud , Mohammed Noor A. M. Abir , Mahmoud M. Kazem , Albarra M. N. Satti , Ali Shebl , Musaab A. A. Mohamed , George Joel Agyemfra , Abdelmajeed A. Elrasheed , Árpád Csámer & Péter Rózsa

To cite this article: Abazar M. A. Daoud , Mohammed Noor A. M. Abir , Mahmoud M. Kazem , Albarra M. N. Satti , Ali Shebl , Musaab A. A. Mohamed , George Joel Agyemfra , Abdelmajeed A. Elrasheed , Árpád Csámer & Péter Rózsa (2025) Comprehensive hazard susceptibility assessment in Port Sudan city using AHP: emphasizing flash flood risk, soil moisture, and salinity dynamics, Geomatics, Natural Hazards and Risk, 16:1, 2593297, DOI: 10.1080/19475705.2025.2593297

To link to this article: https://doi.org/10.1080/19475705.2025.2593297

Published online: 03 Dec 2025.

GEOMATICS, NATURAL HAZARDS AND RISK
2025, VOL. 16, NO. 1, 2593297
https://doi.org/10.1080/19475705.2025.2593297

Taylor & Francis
Taylor & Francis Group

RESEARCH ARTICLE

OPEN ACCESS Check for updates

Comprehensive hazard susceptibility assessment in Port Sudan city using AHP: emphasizing flash flood risk, soil moisture, and salinity dynamics

Abazar M. A. Daoud[a,b], Mohammed Noor A. M. Abir[b], Mahmoud M. Kazem[b], Albarra M. N. Satti[b], Ali Shebl[a,c], Musaab A. A. Mohamed[d], George Joel Agyemfra[a], Abdelmajeed A. Elrasheed[e,f], Árpád Csámer[a,g] and Péter Rózsa[a]

[a]Department of Mineralogy and Geology, University of Debrecen, Hungary; [b]Faculty of Earth Sciences, Red Sea University, Sudan; [c]Department of Geology, Tanta University, Tanta, Egypt; [d]Faculty of Earth and Environmental Sciences and Engineering, University of Miskolc, Hungary; [e]Department of Physical Geography and Geoinformatics, University of Debrecen, Hungary; [f]Department of Geology, University of Khartoum, Sudan; [g]Water Research Center, Red Sea University, Sudan

ABSTRACT

Natural hazards threaten ecosystems, societies, and infrastructure, especially in rapidly urbanizing areas. Port Sudan City, on the Red Sea coast near the Red Sea Hills, is vulnerable to flash floods, soil collapse from salinity, and variable soil moisture, affecting sustainable land use. This study develops a hazard susceptibility assessment using the Analytic Hierarchy Process (AHP) and geospatial analysis. Factors including elevation, slope, curvature, geology, land use/cover (LULC), drainage density, salinity, and soil moisture were integrated into an AHP-based multi-criteria framework. Satellite data (Landsat 8 OLI, Sentinel–2) provided indices such as NDVI, LSE, LST, and SMI. Four factor groups were analyzed: (i) hydro-meteorological factors driving floods; (ii) soil-related factors causing infrastructure damage; (iii) terrain factors increasing rockfall risk; and (iv) LULC and geology-related factors. An integrated hazard map was validated with field surveys and lab analyses. Flood risk had the highest AHP weight, followed by salinity and soil moisture. Southern areas, including the airport and Bashair Terminal, are highly flood-prone; the 2024 Arbaat Dam collapse increased northern flood risk. Shoreline areas face salinity and moisture hazards, while western steep terrain is prone to rockfalls. Results highlight the need for updated hazard maps, better drainage, and sustainable land-use planning.

ARTICLE HISTORY
Received 28 February 2025
Accepted 25 September 2025

KEYWORDS
Analytic hierarchy process; multi-hazard susceptibility mapping; flash flood; soil salinity; soil moisture; Port Sudan

1 Introduction

Over the past decades, geohazards have caused extensive damage to human lives, health, property, infrastructure, environments, and economic activities across the globe (Chelariu et al. 2024; Nagamani et al. 2024; Elomiya et al. 2024; Shu et al. 2024; El baida et al. 2024; Akter et al. 2025; Chwikhi et al. 2025). To reduce these risks, effective geohazard mapping is essential. Integrating a range of environmental, hydrological, and geological factors has been shown to enhance hazard assessment, providing a more comprehensive understanding of catastrophe probability and system flexibility (Gohil et al. 2024; Barman et al. 2024; Zhou and Liu 2024; Ahmad et al. 2025; Ha et al. 2025).

Geohazards refer to natural or human-induced geological processes that present risks to human life, infrastructure, and the environment (Hird et al. 2019; Lee and Griffiths 2024). These include landslides, rockfalls, earthquakes, floods, soil erosion, and collapsing. Such hazards can cause critical socio-economic and environmental effects, particularly in regions with complex topography, weak ecosystems (Vaziri et al. 2018; Ahmed et al. 2019; Saptutyningsih and Dewanti 2023; Lerdsuwankij et al. 2024; Di Salvo et al. 2024; Tesfa 2025; Godes et al. 2025). Despite these apparent risks, a comprehensive geological hazard assessment for Port-Sudan has yet to be conducted. With the city's increased extension from both natural and human-induced factors, there is a crucial need for a detailed understanding of its geological vulnerabilities. This

CONTACT Abazar M. A. Daoud abazar.daoud@science.unideb.hu

research aims to fill this gap by developing a geohazard risk map for Port Sudan city, focusing on the critical risks of flooding, soil instability, and other geological threats using GIS-based multi-criteria decision analysis (MCDA) and analytic hierarchy process (AHP).

MCDA, and in particular AHP, is widely applied in geosciences for integrating multiple factors in decision-making. For example, it is used in groundwater potential mapping to assess parameters such as rainfall, geology, and drainage density to identify suitable groundwater zones (Ma and Mei 2021; Shebl et al. 2022; Zou et al. 2023; Agogue Feujio et al. 2024; Nagamani et al. 2024; Patel et al. 2024; Lavanya and Muthukumar 2024). For mineral exploration, it highlights areas based on geochemical anomalies and lithology (Akinlalu et al. 2024; Abubakar et al. 2025). It is also applied in landslide susceptibility mapping by analyzing slope, soil type, precipitation, and seismic activity (Panchal and Shrivastava 2022; Akter et al. 2025; Badavath and Sahoo 2025; Tavakoli et al. 2025; Abdelkader and Csámer 2025; Chwikhi et al. 2025; Dieno and Pathan 2025). Given its effectiveness in these domains, AHP is a powerful tool for hazard susceptibility assessment, as it systematically integrates environmental, hydrological, human, and geological factors to optimize hazard improvement and land-use planning (Huang et al. 2023; Zhang et al. 2025; Tavakoli et al. 2025; Ashfaq et al. 2025; Chwikhi et al. 2025; Ferreira et al. 2025), particularly in Sudan, where such studies remain limited.

Port Sudan, one of the largest cities in Sudan, plays an important role in regional and international trade due to its strategic location on the Red Sea coast. As the main port for Sudan's import and export activities, the city has become of additional importance among ongoing political shifts, recently appearing as the capital of the Sudan. However, its coastal location, linked with rapid population growth and urban expansion (from about 397,000 in 2014 to over 547,000 in 2024) (DeSA 2013; Hawash et al. 2021; Cangiano 2024; Brakman et al. 2025), has led to significant structural and environmental challenges that cause serious risks to its sustainability and development.

The city is situated between the Red Sea Hills to the west and the Red Sea itself, creating a unique geographical setting that contributes to its susceptibility to geohazards. Among the most critical risks are floods, soil salinity, and soil moisture which occur frequently due to the seasonal passing of water from the surrounding basement terrains in the west towards the coastal areas in the eastern part. This natural geohazard is increased by human activities, including artisanal mining and soil excavation along flood channels, which disturb the natural landscape, destabilize soil conditions, and increase the likelihood of floods. These issues also signify public health, as they contribute to water pollution and the degradation of local ecosystems. Despite its strategic importance, Port Sudan faces critical challenges in risk management and sustainable land-use planning. Rapid urban expansion (now exceeding 600,000) has occurred without adequate consideration of flood-prone zones, soil salinity impacts, or moisture-related instability. Drainage infrastructure is limited and outdated, leaving major facilities increasingly vulnerable to flash floods. In addition, shoreline development has intensified exposure to soil salinity and moisture, accelerating infrastructure deterioration. These issues highlight the absence of updated hazard susceptibility maps and effective land-use regulations, making it difficult for planners and decision-makers to implement preventive measures. Addressing these gaps is therefore essential for the city's long-term sustainability. Applied scientific researches are vital for understanding environmental phenomena and mitigating the effects of human activities. By integrating interdisciplinary approaches, including earth sciences, engineering, and medical research, a comprehensive analysis can be achieved to address pressing environmental challenges such as artisanal mining impacts, industrial waste, and plastic pollution.

The primary objectives of the present study are, for the first time in this area, to develop a hazard susceptibility map by integrating multidisciplinary data using MCDA and AHP, validated through field observations and laboratory analyzes, and to provide actionable recommendations for effective risk management and sustainable land-use planning. In this study, eleven critical factors were incorporated into the AHP framework, grouped into four main categories that strongly influence hazard susceptibility: (i) hydro-meteorological factors (rainfall, slope, drainage density) contributing to flash flood hazards; (ii) soil-related factors (salinity and soil moisture) causing infrastructure damage and ecosystem degradation; (iii) topographic conditions in the Red Sea Hills increasing rockfall susceptibility; and (iv) LULC with geology related factors and an integrated multi-hazard assessment combining all factors into a comprehensive susceptibility map.

2 Physiographic features of the study area

The study area is located in the eastern part of Sudan within the Red Sea state, extending between the longitudes 30°36' and 30°37', and latitudes 18°30' and 20°. The region covers an area of 16,000 square kilometers, extending to 160 kilometers in length and 100 kilometers in average width (Figure 1a).

The study area is connected to the base of Sudan through the main roads and railways that link other cities to Port-Sudan. The importance of the city is further highlighted as a destination for petroleum exports, with the Bashair Port for oil exports located near the international airport. This boosts the region's position as a strategic focal point for trade and transportation in eastern Sudan (Figure 1b).

The study area represents a variety of different landforms, including mountains, valleys, and seasonal streams, with distinguished geographical features such as the Red Sea Hills, the coastal plain, the Red Sea itself, and a complex drainage system. The Red Sea Hills, running parallel to the coast, are main sources of freshwater and rich in economic resources like gold, manganese, marble, barite, gypsum and limestone (Whiteman 1970; Kenea et al. 2001; Martin Williams 2019; Abu-Fatima et al. 2021). The coastal plain, widening along the Red Sea, is vital for salt production and holds major ports, free zones, and tourist marinas. The Red Sea, a 1,932-kilometer-long basin, connects the Indian Ocean to the Mediterranean and is surrounded by arid deserts but features rich biodiversity (Bosworth 2015). The region's drainage system, shaped by geological structures, includes over 12 wadis and khors that provide essential water resources for cities like Port Sudan and Suakin, supported by dams and groundwater reservoirs. The area has a hot desert climate (BWh according to the Köppen's classification), with humid summers and mild winters, sees annual temperatures averaging 28.4 °C, high humidity in summer, and limited rainfall (76 mm annually) concentrated between August and January (Köppen 1900; Kottek et al. 2006; Beck et al. 2018).

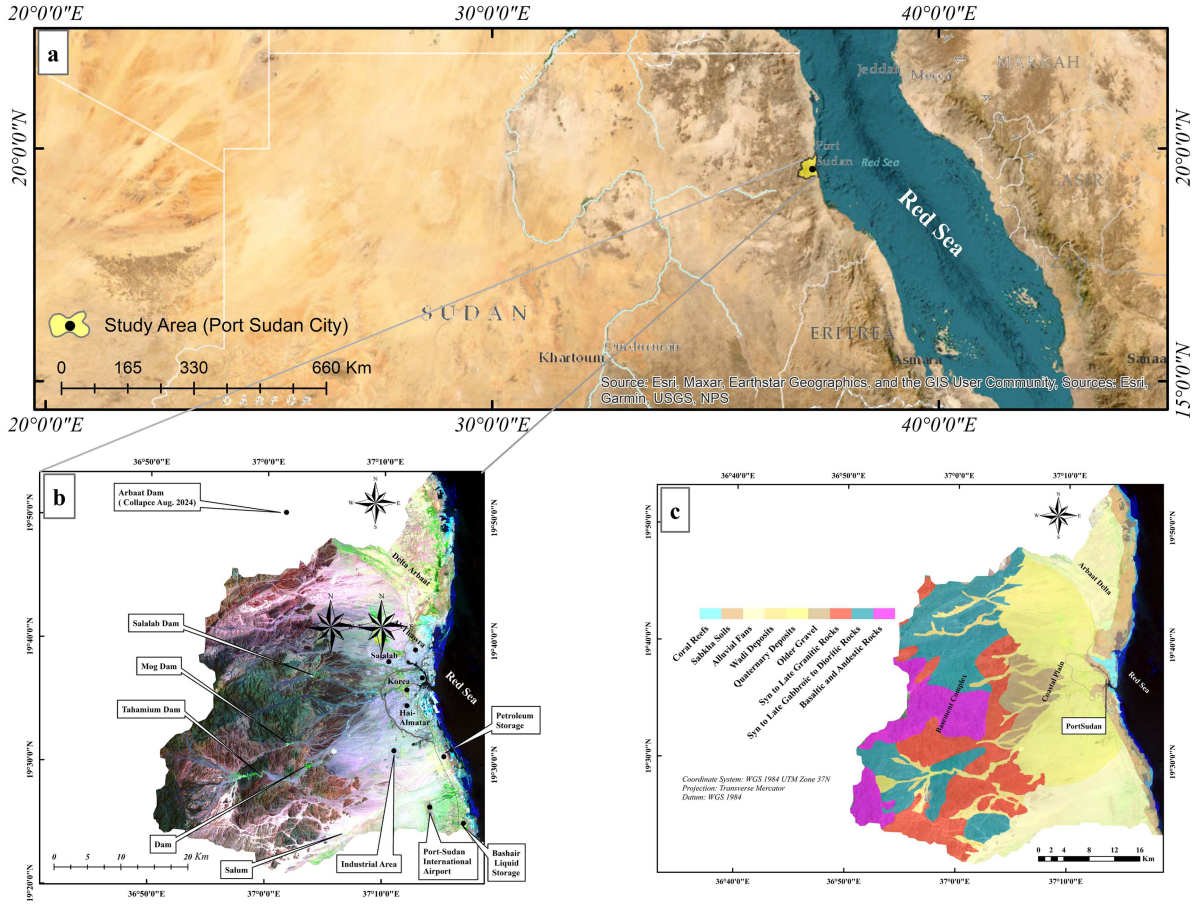

Figure 1. (a) Location map of the study area; (b) RGB map showing major physiographic features of the Port Sudan City; (c) Simplfied geoological map of the study area.

Geologically, the basement complex of the Red Sea Hills spreads over large areas in northeastern Sudan and is characterized by different degrees of metamorphism, which includes meta-volcano sedimentary sequences interspersed with extrusive and intrusive igneous complexes. Igneous rocks of indeterminate thickness, such as weathered granite and diorite rocks largely cover the area. Metavolcano-sedimentary sequences completely surrounded by older rocks of amphibolite facies exposed in the northern and southern regions of the Red Sea Hills in the western part (Stern et al. 1989; Elsamani et al. 2001; Kenea et al. 2001; Elsayed Zeinelabdein et al. 2021).

Nubian Sandstone Formation (NSF) was deposited in various continental environments during the Cretaceous period. Along the coastal plain, NSF is mixed with other marine sediments, especially near the coastal area. Cenozoic sediments occur above the basement rocks in the form of unconformity and comprise six major formations based on their rock types and fossil content (Bosworth 2015; Laurila et al. 2015; Babikir et al. 2021). They are overlain by the most recent sedimentary formations belonging to the Quaternary period, representing sediments deposited in continental, transitional, and marine environments. Most of them are Pleistocene deposits along the Red Sea coast, consisting of complex coral sediments and coral reefs of more than 16 meters thick, found both above the waterline and extending several kilometers into the islands. Sabkha (salt flats) deposits are found in different areas along the coastal plain adjacent to the Red Sea (Youssef El Sayed 1991; Loughland 2018). The recent deposits found in streams and drainage basins. The wadi systems along the coast form a series of fans and deltas composed of gravel, silt, and clay (Figure 1c).

3 Data and methodology

3.1 Data acquisition

The datasets were categorized into four main groups to ensure a full analysis of hazard susceptibility. These categories include:

a) ***Geology and Soil Datasets:*** This group includes key geological properties such as lithology, soil type, soil moisture, and salinity, which are essential for identifying the geological and structural attributes of the study area.
b) ***Topographic Data:*** Derived from a Digital Elevation Model (DEM), this group includes slope, curvature, and elevation data, which are important for evaluating terrain variability and its influence on hazard mechanisms.
c) ***Hydrological Data:*** This data focuses on water-related parameters, including flow accumulation, stream networks, drainage density, and watershed boundaries, explaining the hydrological processes and their effect on hazard susceptibility.
d) ***Climatological Factors:*** Climate-related variables such as rainfall, humidity, and temperature are incorporated to evaluate the impact of climatic conditions on the study area.

The datasets utilized in this research were sourced from different platforms and methods including satellite imagery, topographic maps, elevation, and thematic layers such as LULC, rainfall, salinity, temperature, soil moisture, and humidity (Table 1, Figure 2). Additionally, field surveys and laboratory analyzes were integrated to ensure the accuracy and comprehensiveness of the data.

3.2 Data preprocessing and index calculation

In the first analytical stage, GIS software was utilized for data conversion; transforming digital maps from vector to raster format, and Spatial Analysis tools such as distance analysis and reclassification were applied to assess spatial relationships among variables. Satellite imagery from **L8 OLI/TIRS** and **S2 MSI** was used in this study. The salinity index (SI) was calculated using different formulas suggested by (Elhag 2016), where the Land surface temperature (LST) helps to distinguish moist zones and high-salinity areas (such as sabkha environments near the shoreline) was calculated from L8 thermal bands (Avdan and

Table 1. Data used in the present study.

Data	Source	Date	Thematic map	Resolution/Scale
Geology and Litholog	Geological Research Authority of Sudan (GRAS)	2018	Geological Map	1:250:000
ASTER	NASA METI/ERSDAC https://lpdaac.usgs.gov	2019	DEM Drainage Slope Aspect Curvature	30m
L9	USGS www.earthexplorer.usgs.gov	2024	RGB Salinity Soil Moisture	30m
LULC	ESRI www.earthexplorer.usgs.gov ArcGIS Living Atlas of the World https://livingatlas.arcgis.com/landcoverexplorer/	2024	LULC Maps	10m
Soil Map	FAO www.fao.org	2019	Soil Map	1:250:000
Climate data	www.crudata.uea.ac.uk	2022\2024	Rainfall and flooding	0.25° (25 km)
Watershed	www.hydrosheds.org	2019	Watershed	30m
Rainfall	PERSIANN-CCS https://chrsdata.eng.uci.edu	2016 2024	Rainfall Map	0.04° (~4 km)

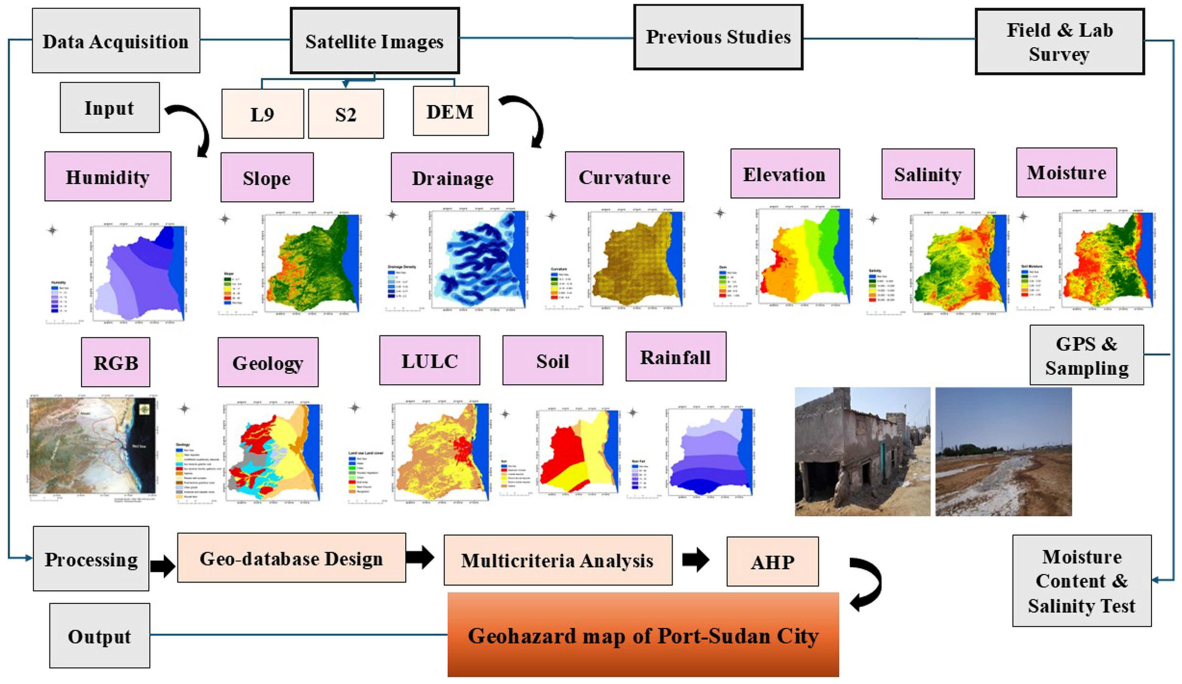

Figure 2. Flowchart illustrates the methodology for creating a geohazard map based on spatial data and AHP.

Jovanovska 2016; He et al. 2019; Vanhellemont 2020; Niclòs et al. 2021) Additional indices, including NDVI, LSE, and SMI, were also derived from L8 and S2 datasets, ensuring a comprehensive integration of remote sensing parameters, as outlined in the steps below:

1) *Conversion to top atmosphere (TOA) radiance*

$$L(\lambda) = ML\, x\, Band10 + AL - Oi \quad (1)$$

where L(λ): TOA spectral radiance; ML: Radiance multiplicative band (from MTL txt); AL: Radiance adds band 10 (from MTL txt); and Oi: correction value (for Landsat 8 Band10 its = 0.29).

2) Kelvin (k) to Celsius degree C°

$$BT = K2 / \ln(k1/L(\lambda) + 1) - 273.15 \quad (2)$$

$$BT = (1321.0789 / Ln(774.885 / "TOA" + 1)) - 273.15 \quad (3)$$

where: BT: Top of Atmosphere brightness temperature C°; L(λ): TOA spectral radiance; K1: K1 constant for band10 (from MTL txt); K2: K2 constant for band10 (from MTL txt).

3) *Normalized Difference Vegetation Index (NDVI) calculation*

$$NDVI = (NIR - RED) / (NIR + RED) \tag{4}$$

4) Land Surface Emissivity (LSE)

$$PV = ((NDVI - NDVI_{min}) / (NDVI_{max} - NDVI_{min}))^2 \tag{5}$$

where: PV: Portion of Vegetation; NDVI: values of NDVI image3; NDVI max/min: Max & Min values of NDVI image.

$$E = 0.004 * PV + 0.986 \tag{6}$$

Where: E: Land Surface Emissivity; PV: Portion of Vegetation.

5) Land surface temperature (LST)

$$LST = BT/ (1 + (\lambda * BT/C2) * \ln (E)) \tag{7}$$

where: BT: Top of Atmosphere brightness temperature C°; λ: Wavelength of emitted radiance; for Landsat 9 Band10 $\lambda = 10.8$ and for Band11 $\lambda = 12$; E: Land Surface Emissivity:

$$C2 = h * c/s\, C2 = 14388mK \tag{8}$$

h: Plank's constant = $6.626 * 10^{-34}$ mK; s: Boltzmann constant = $1.38 * 10^{-23}$ JK; c: velocity of light = $2.998 * 10^{8}$ m/s

6) *Soil moisture index (SMI)*

$$SMI = (LST_{max} - LST) / (LST_{max} - LST_{min}) \tag{9}$$

After preprocessing and calculating the various parameters, all factors were reclassified into three major categories (high, medium, and low) based on their relative contribution to hazard susceptibility and to provide clarity on how each factor contributes to hazard susceptibility. The criteria for defining the ranges of these classes were derived from a combination of (i) threshold values and classification schemes reported in previous hazard susceptibility studies in similar areas (Rashwan et al. 2024), and (ii) the specific environmental and geomorphological characteristics of the Port Sudan region. For example, slope and drainage density thresholds were adapted from regional flood susceptibility but refined to reflect the steep terrain of the Red Sea Hills, while salinity and soil moisture ranges were informed by field/laboratory observations in the study area. This hybrid approach ensured that the classification was both scientifically consistent with established methods and tailored to the local context. Once reclassified, the factors were assigned weights through the AHP pairwise comparison process, reflecting their relative importance in influencing hazard risks.

The classification considered both literature benchmarks (e.g. rainfall thresholds, slope gradients, soil salinity levels) and the unique characteristics of the study area. This approach ensures that the relative impact of each factor on hazards such as flash floods, soil instability, and rockfalls is explicitly quantified. The reclassified factors were then assigned weights according to their relative importance in contributing to different hazard risks.

3.3 Analytic hierarchy process (AHP)

The AHP, developed by Saaty (1987), is a structured decision-making tool used to analyze complex problems by breaking them down into a hierarchy of simpler components. The AHP method was used to assign weights to each factor based on its relative importance, especially in geohazard susceptibility

mapping (Obiegbu 2021; Panchal and Shrivastava 2022; Mao et al. 2024; Tesfa 2025). Pairwise comparisons were conducted, and consistency ratios were calculated to ensure the reliability of the weights.

In this study, AHP was used to evaluate the relative importance of factors influencing geohazard susceptibility, such as slope, rainfall, soil type, and land use. The weights derived from AHP were integrated with GIS to create a geohazard susceptibility map, which was validated using field and laboratory data (Figure 2).

Criteria layers were prepared using ArcGIS software. These layers were converted to a raster format and resampled, then reclassified based on their impact. The weights of the criteria were determined using the AHP method to identify geological hazard locations. After classifying the layers and determining the weights of the criteria, the layers were combined by applying the AHP-derived weights. The combination was performed using the Weighted Overlay Tool in ArcGIS to produce the final geohazard map according to the following Equation (10):

$$Si = (Rw*Rr + SLw*SLr + DDw*DDr + SMw*SMr + Ew*Er + Aw*Ar + Sw*Sr + LUw*LUr + Gw*Gr + SAw*SAr) \quad (10)$$

where **Si**: the number of potential hazard sites; **w**: weight of each criterion; **r**: rating for each criterion; **R**: Rainfall; **SL**: Slope; **DD**: Drainage Density; **SM**: Soil Moisture; **E**: Elevation; **A**: Curvature (direction); **S**: Soil; **LU**: Land Use; **G**: Geology; and **SA**: Salinity.

The method began with the formulation of a hierarchical structure, where the ultimate goal was hazard susceptibility mapping, the intermediate level consisted of the selected criteria, and the bottom level represented the spatial alternatives. Each factor was subjected to pairwise comparison using Saaty's fundamental scale (1–9), whereby expert judgments were elicited to determine the relative importance of one factor over another (e.g. the higher influence of slope compared to soil type in slope-instability processes). The comparison matrix was normalized and processed using the eigenvalue method to derive a set of weights that quantify the contribution of each factor to the overall hazard susceptibility. In the GIS environment, all thematic layers were prepared from available datasets, reclassified into ordinal susceptibility classes (e.g. slope categories or rainfall intensity ranges) and standardized to a common scale. The AHP-derived weights were then applied to these reclassified layers through a weighted linear combination approach, producing a composite hazard index that was further classified into susceptibility zones (low, medium, and high).

3.4 Validation and sensitivity analysis

3.4.1 Pairwise comparison matrix

To quantify the relative importance of the selected factors in hazard susceptibility, a pairwise comparison matrix was constructed following Saaty's scale. Each factor was compared with others based on expert judgment, literature review (Ullah et al. 2024; Bedada and Dibaba 2025), and the specific characteristics of the study area. The matrix includes hydro-meteorological factors, soil-related factors, topographic factors, geology, and land use/cover. The total values of each column were normalized to calculate the weight of each factor, ensuring that the sum of all weights equals 1. To verify the reliability of these subjective judgments, the Consistency Ratio (CR) was calculated and confirmed to be within acceptable limits ($CR \leq 0.1$) (Saaty 1987; Malczewski and Rinner 2015) (Equations (12), (13), and ((14))). This process ensures a transparent and reproducible determination of factor weights for the AHP-based hazard susceptibility assessment. Our methodology combined field observations and laboratory results with spatial analysis, ensuring a robust and scientifically grounded evaluation of geohazard risks. The evaluation incorporated 11 critical factors (elevation, slope, curvature, rainfall, drainage density, flow accumulation, geology, soil, LULC, salinity, and soil moisture), with a particular focus on five primary contributors: flood risk, soil salinity, moisture, geology, and LULC.

$$\tilde{A}_{ij} = \frac{A_{ij}}{\sum_{k=1}^{n} A_{kj}} \quad (11)$$

where: A_{ij}: is the original value in row i, column j; A_{kj}: is the sum of all elements in column j; and $\tilde{A}_{ij}$: is the normalized value.

$$CR = \frac{CI}{RI} \tag{12}$$

Where:
RI (Random Index) is a predefined value based on n. For $n = 11$, RI = 1.51; CI: Consistency Index.

$$CI = \frac{\boldsymbol{\lambda_{max}} - \mathbf{n}}{n - 1} \tag{13}$$

where: $\boldsymbol{\lambda_{max:}}$ is the average of the weighted sum vector divided by the priority vector.
n: is the number of factors which calculated using (Equation (14)):

$$\boldsymbol{\lambda_{max,i}} = \sum_{j=1}^{n} A_{ij} * w_j \tag{14}$$

3.4.2 Sensitivity analysis

Sensitivity analysis was carried out in order to produce important information on the influence of rating values and weights assigned to each factor (Gogu and Dassargues 2000); map removal sensitivity analysis is used in this study to determine the sensitivity of the final geohazard map by removing one factor at each generation of the geohazard map (Becker 2006; Gau et al. 2006; Gholizadeh et al. 2017; Allafta et al. 2021; Arabameri et al. 2021) applied different techniques to define and assess map removal sensitivity analysis and they used the following expression (Equation 15):

$$s_{ix} = \frac{P_i}{N} - \frac{Px_i}{n} \tag{15}$$

where S_{ix} is sensitivity associated with the removal of one map of parameter X, P_i is the computed potential value of the cell or the area, P_{xi} is the potential value of the cell or the area after excluding parameter X. N is the total number of used parameters for computing potential value of the cell or the area, n is the number of used parameters for computing potential value of the cell or the area after excluding one parameter.

3.4.3 Field surveys and sampling

Several field surveys were conducted to identify areas with high flood risks, salinity, and soil moisture conditions. During these surveys, soil samples were systematically collected from various locations across the study area for subsequent laboratory analysis to assess their physical and chemical properties. Observations were also made to evaluate the effects of soil moisture and salinity on different construction buildings, including their potential to weaken foundations and contribute to structural collapsing. This provided the spatial distribution of geohazards and their impacts on both natural and construction environments.

4 Results

4.1 Factors of hazard susceptibility mapping

4.1.1 Geology and soil

The geology of the study area is characterized by different lithological units. In the west, it consists of basement complex rocks, while the central region features Quaternary and recent deposits. Near the coastal plain, the geology is dominated by limestones of varying thickness and depth. Additionally, the

marine sediments of the Quaternary period and the present period include coral reefs, sabkha deposits, and sandstone covering the area behind the shoreline (Figure 3a).

Geology plays a crucial role in determining geohazard susceptibility. In the western region, RSH are dominating, forming high-relief terrains that are highly susceptible to rockfalls and slope instability. In contrast, the central region, characterized by Quaternary and recent deposits, is more susceptible to flooding and soil erosion due to its loose and unconsolidated soil. Closer to the coastal plain, the presence of limestone formations of varying thickness influences groundwater flow and contributes to karst-related subsidence hazards. Additionally, the sabkha deposits in areas behind the shoreline, particularly east of Port Sudan, are highly susceptible to salinity-induced degradation.

Due to the limited availability of previous soil mapping studies in the region, a comprehensive soil map was developed by integrating field observations with data from the Food and Agriculture Organization of the UN (FAO) (www.fao.org). However, since the FAO soil map lacks classification for sabkha soils, field-based assessments were essential for refining soil classifications. The final map identifies four major soil types: older gravels (originating from the basement complex), Quaternary deposits, sabkha soils, and coral reef limestone, which are primarily distributed along the shoreline (Figure 3b).

Given the scarcity of prior soil mapping studies in the area, a soil map was developed. The present study identified four major soil types that contributes the geohazard susceptibility mapping (Table 2).

4.1.2 Soil salinity and moisture

The study area is characterized by high salinity (red color on map in Figure 3c), which contributes to several hazards such as degraded soil structure, reduced vegetation cover, and exacerbated erosion and waterlogging. Similarly, excessive soil moisture (red color on map shown by Figure 3d) weakens soil

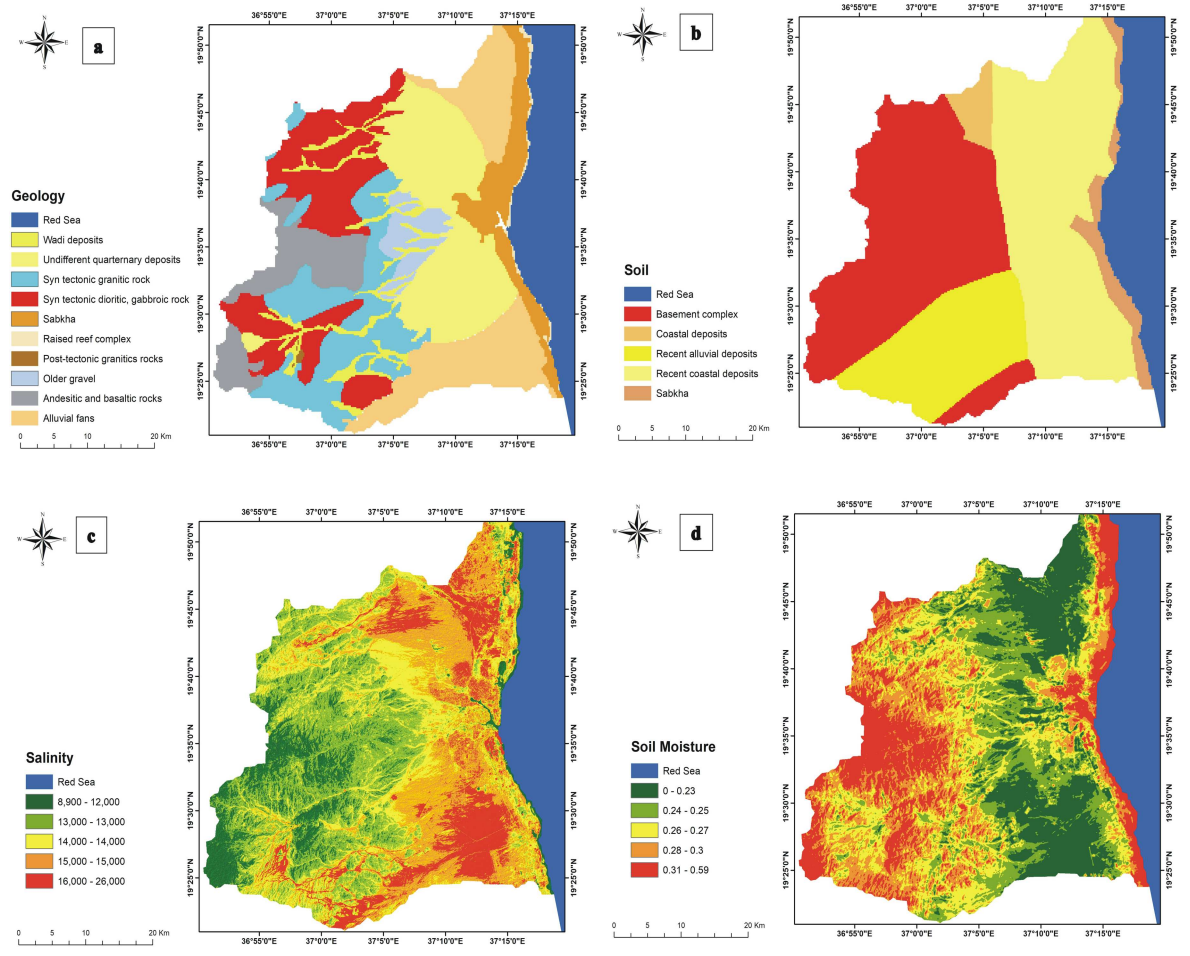

Figure 3. (a) Geological map of the study area; (b) soil map; (c) salinity index; (d) soil moisture index.

Table 2. Soil types and associated geohazard susceptibility in the study area.

Soil type	Location	Properties	Geohazard	Examples
Older gravel	Western part	Derived from basement complex, relatively stable	Stable but Susceptible to flash flood runoff due to high elevation	Salum, Alexandria, Al-Eskan
Quaternary deposits	Central region	Unconsolidated sediments	Stable	Hai-Almatar, Dar Alsalam, Dar Alsafa, Industrial area,
Sabkha soil	Coastal plane	High salinity, moisture content	Leads to infrastructure damage, collapsing	Salalab 6, Barcelona, Deim Alnoor, Althawra, Falamingo, Alkilo, Korea
Coral Limestone	Shoreline	Marine derived sediments	At risk of coastal erosion and collapsing	City center, Abu-Hashish, Transit, Ports

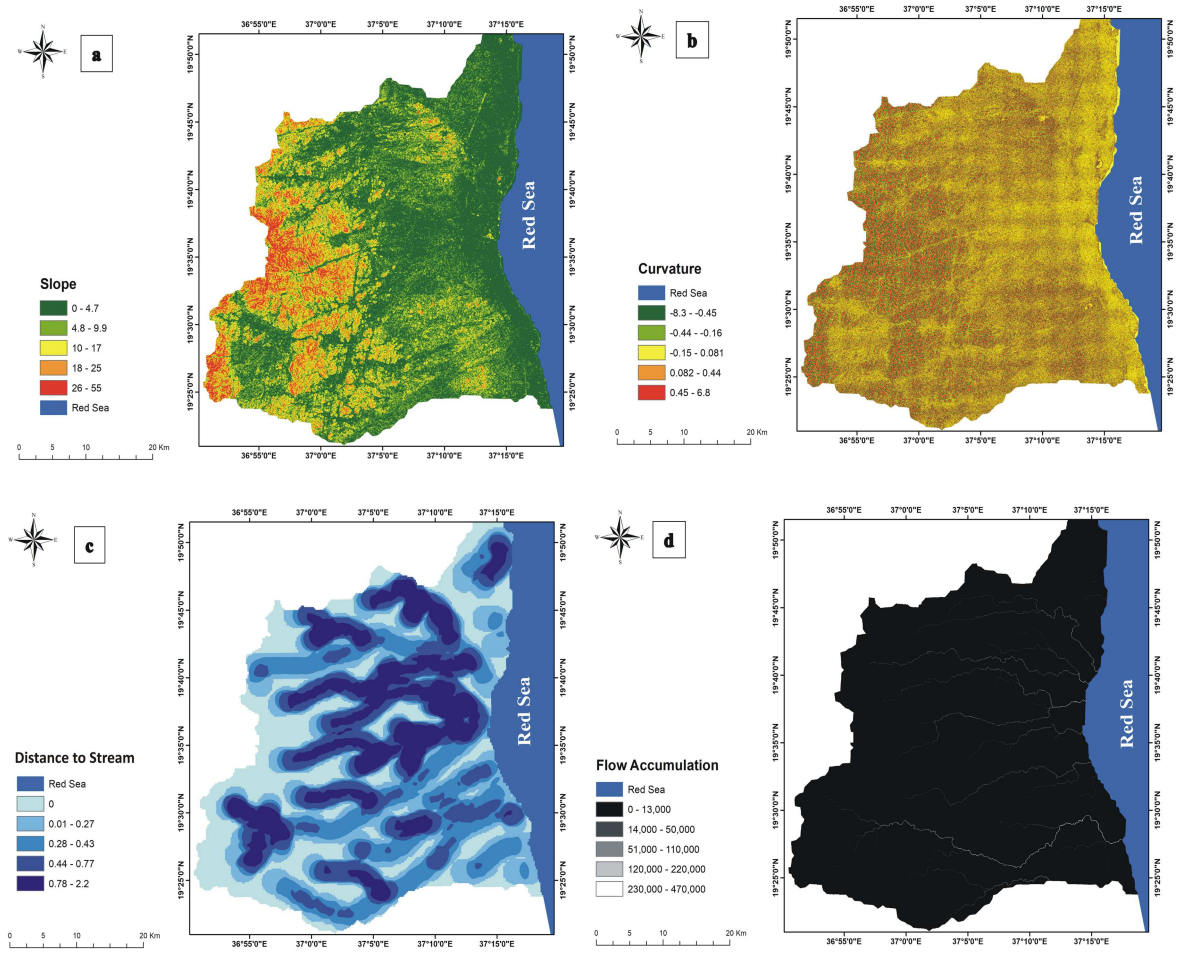

Figure 4. (a) slope; (b) curvature; (c) drainage density; (d) flow accumulation map.

strength, leading to structural settling and collapsing. Fluctuations in moisture levels can also cause shrink-swell behavior, damaging infrastructure like foundations and roads.

4.1.3 Topographic/terrain

The study area exhibits different topography, ranging from steep slopes to gentle inclines and flat terrain, influencing geohazard susceptibility (flash flood, soil salinity, and moisture). Steep slopes, primarily in the western part (red color in map shown in Figure 4a), are highly susceptible to rockfalls due to gravity-driven mass movement, exacerbated by fractures and weathering. In contrast, coastal areas, particularly in the central and eastern parts near the shoreline (light and dark green), are highly susceptible to flooding. These areas experience water accumulation due to their lower elevation, poor natural drainage, proximity to water bodies, and predominantly flat terrains. Curvature, a key factor in surface flow patterns and

erosion susceptibility, further defines terrain stability. Positive curvature values indicate hilly terrains in the west (red), where runoff is rapid, increasing erosion risks. Negative values correspond to valleys and depressions (yellow), which represent as natural drainage basins, accumulating water and intensifying flash flood hazards. Flat surfaces, with curvature values near zero (green), dominate the coastal plain and central regions, contributing to extended water retention and salinity accumulation. These topographic influences are visually represented in Figure 4a and 4b.

4.1.4 Hydrology

Because of the flood risk in the study area is the major risk related to water parameters, including flow accumulation, stream networks, distance to stream channels, and watershed boundaries. Firstly, we choose three watersheds that cover our study area and then we generate maps of hydrological factors.

The drainage density map particularly distance to stream (Figure 4d) reveals significant spatial variability across the study area. High drainage density is concentrated in the central regions (Port Sudan) with steep slopes and impermeable geological formations, primarily in different districts in the study area such as (Deim Alnoor, Salalab, Hay Almatar, Barcelona, and Alkilo) and in the southern part of the study area (Port-Sudan Airport, Bashair Oil Storage) (see Figure 1c) which suggests a well-developed drainage network. These areas experience rapid surface runoff, increasing susceptibility to flash floods during heavy rainfall. Conversely, regions with low drainage density, predominantly located in flatter or permeable zones, exhibit slower water drainage, reducing the likelihood of rapid runoff events.

The hydrological factors align closely with the curvature and slope distributions, indicating a strong topographic control. These findings highlight the importance of incorporating drainage density as a key parameter in geohazard assessments, particularly identifying areas vulnerable to flooding and erosion (Figure 4b).

To enable geohazard susceptibility analysis, all conditioning factors were systematically reclassified into three susceptibility classes (high, medium, low). This step ensured that heterogeneous datasets, ranging from topographic indices to land use and soil types, were standardized into a common framework. The classification criteria and ranges for each factor are summarized in Table 3.

Table 3. Reclassification of geohazard factors into susceptibility classes.

Factor	Units	Low (Score = 1)	Medium (Score = 2)	High (Score = 3)	Rationale
Elevation (DEM)	m a.s.l.	>50 m (uplands, well-drained)	20–50 m (moderate plains)	0–20 m (low-lying coastal plains)	Lower elevations accumulate runoff, increasing flood and salinity hazards.
Slope	degrees	0–5° (flat plains, slow runoff)	5–15° (moderate slopes)	>15° (steep slopes)	Steeper slopes favor rockfall & erosion; flat plains trap water & salinity.
Curvature	–	Convex (>0.05)	Flat (−0.05 to 0.05)	Concave (<−0.05)	Concave → water concentration; flat → ponding/salinity; convex → runoff/ erosion.
Distance to stream	km/km^2	<2	2–4	>4	Dense drainage networks channel floods rapidly.
Flow accumulation	upstream cells	<50	50–200	>200	Higher accumulation = stronger flood pathways.
Rainfall	mm/year	<100 (arid NE zones)	100–250	>250 (SW highlands)	More rainfall increases flash flood & erosion risk.
Soil	Class	Weathered basement gravels (permeable)	Alluvial/ Quaternary deposits	Sabkha soils & recent coastal deposits	Sabkha → salinity + instability; Quaternary → loose, flood-prone; basement gravels more stable.
Soil salinity	dS/m	<2	2–4	>4	High → soil degradation, sabkha formation, foundation damage.
Soil moisture	% (surface index)	<10	10–20	>20	High moisture → swelling/shrinkage, settlement, waterlogging.
Geology	Lithology	Competent basement rocks	Limestones (karst-prone)	Quaternary/sabkha/ evaporites	Weak, soluble, or unconsolidated lithologies amplify hazards.
LULC	Classes	Forest/vegetation cover	Cropland/ rangeland	Built-up, bare ground, sabkha, flooded vegetation	Impervious & bare → high runoff; sabkha → salinity/instability.

4.1.5 Elevation

Elevation plays a critical role in hazard susceptibility in Port Sudan and its surroundings. The Red Sea Hills in the western part of the study area reach elevations of about 620–1300 m, while the coastal plain near the Red Sea ranges from 0–35 m (Figure 5c). These elevation gradients strongly influence the spatial distribution of hazards. Higher elevations are directly linked to flash flood generation, as steep slopes accelerate runoff and increase stream power. In contrast, the low-lying coastal plains act as natural flood-receiving zones, where water accumulates and amplifies flood susceptibility. Additionally, the very low elevations along the coast are highly sensitive to salinity intrusion and soil moisture variations due to the proximity of seawater and shallow groundwater tables.

4.1.6 Climate

Rainfall, temperature, and humidity are important factors in geohazard susceptibility mapping (Shou and Lin 2020; Xu et al. 2024; Semnani et al. 2025). The rainfall map (Figure 5a) indicates that precipitation is unevenly distributed across the study area. Higher rainfall values are concentrated in the southwestern part, typically coinciding with elevated terrains, where orographic effects are prominent. These areas are more susceptible to flash floods and soil erosion due to increased runoff. In contrast, lower rainfall is observed in the northeastern part, where arid conditions prevail, resulting in limited surface water flow and a reduced likelihood of flood-related hazards.

The humidity map shows a strong correlation with proximity to the Red Sea, with higher humidity values in coastal regions and lower values inland (Figure 5b), whereas the temperature distribution indicates significant spatial and seasonal variability. Higher temperatures are concentrated in lowland

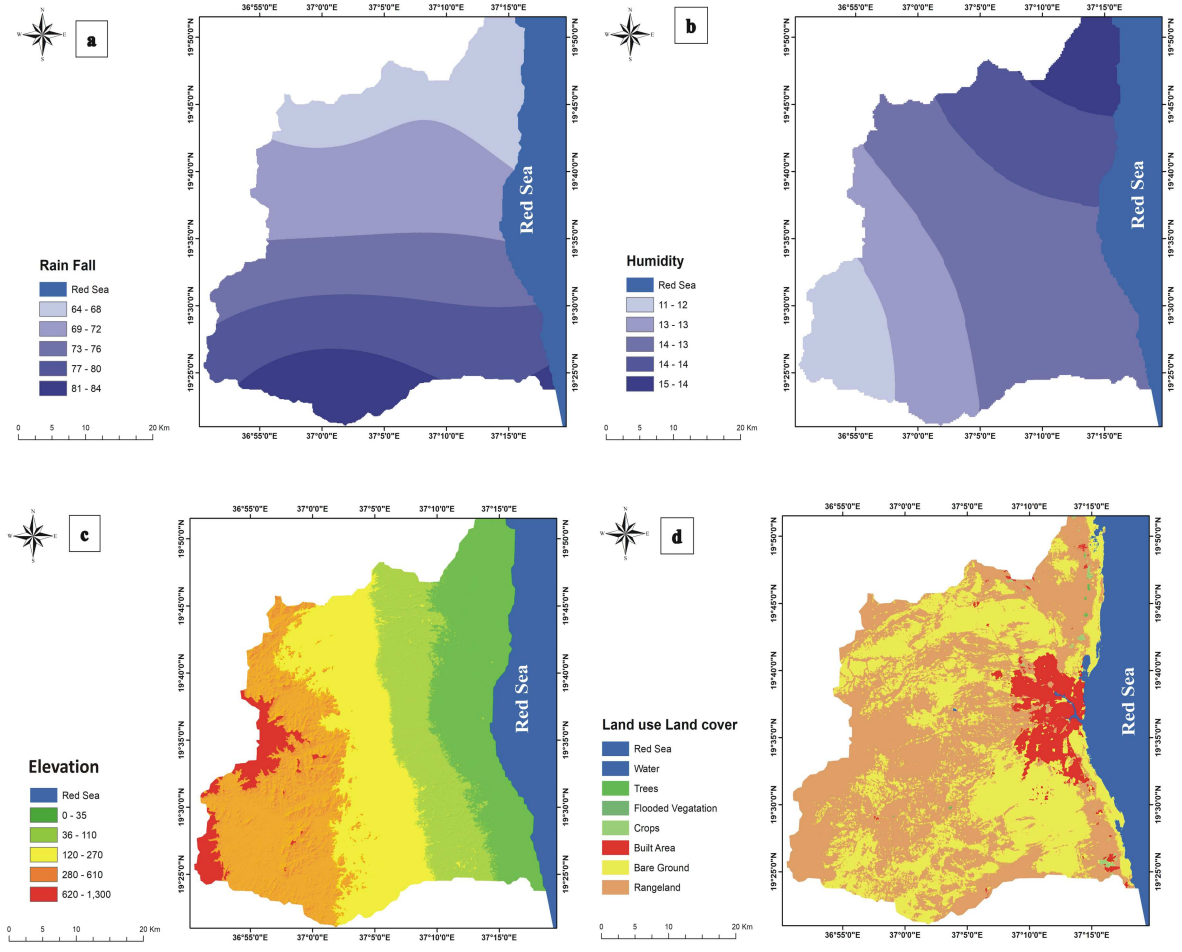

Figure 5. (a) Rainfall map; (b) humidity; (c) Elevation map, (d) an updated LULC map of 2024.

and inland regions, where intense heating can lead to soil destruction, increasing vulnerability to wind erosion.

4.1.7 Land use and land cover (LULC)

The human element significantly influences geomorphological studies in the area, particularly through urban development and tourism. Based on recent study done in our study area (Hawash et al. 2021). The analysis of high-resolution satellite imagery demonstrates how human activities modify the landscape, often without sufficient awareness of potential environmental impacts. Understanding this relationship through remote sensing techniques is crucial for sustainable decision-making.

The LULC map highlights the distribution of various land types in the study area, including built-up areas, bare ground, rangeland, crops, forests, flooded vegetation, and water bodies. Built-up areas are prone to urban flooding due to impervious surfaces, while bare ground and rangelands are at risk of erosion, especially on slopes or during heavy rainfall. Croplands are vulnerable to both flooding and drought, impacting agriculture, while flooded vegetation zones and coastal areas near the Red Sea are highly susceptible to inundation. Forested regions help stabilize soil and reduce erosion risks, while water bodies indicate potential flood sources. This LULC map is vital for identifying geohazard-prone zones and planning mitigation strategies (Figure 5c).

While each factor has its own distribution and reclassification scheme, their relevance differs depending on the type of hazard. For instance, slope gradients and elevations are a key determinant for flash flood intensity, but they play a relatively smaller role in salinity accumulation. The role of each factor in relation to the three major hazards considered (flash floods, soil salinity, soil moisture) is synthesized in Table 4.

4.2 MCDA and AHP

In this study, the AHP was employed to evaluate hazard susceptibility mapping particularly focusing on the most important hazard caused in the study area depending on each factor (hydro-meteorological, topographical/terrain, soil related factors, and LULC with geological factors) by integrating geological, hydrological, environmental, topographical, and human factors. Eleven main criteria—elevation, curvature, slope, flow accumulation, rainfall, distance to stream channels, soil types, salinity, soil moisture, geology, and land use/land cover (LULC)—were weighted based on their contribution to hazard susceptibility, with flood risk receiving the highest weight, followed by salinity, soil moisture, geology, and LULC.

These factors were reclassified into three susceptibility classes (high, medium, and low) based on their respective characteristics and influence on geohazards (Table 3). The classification process utilized different techniques designed for each factor. For instance, geology, soil, and LULC were classified manually based on previous studies, field observations, and the Natural Breaks (Jenks) method.

Table 4. Influence of factors on major hazards in Port Sudan city.

Factor	Flash flood susceptibility	Salinity & moisture-related hazards	Rockfall & terrain instability
Elevation	Lowlands trap floodwater	Coastal plains promote salt accumulation	High elevations linked to slope instability
Slope	Steep slopes → faster runoff	Flat slopes → ponding & salinity buildup	Steep slopes drive rockfalls, mass movement
Curvature	Concave → concentrated flows	Flat → long-term ponding & salinity	Convex breaks promote localized failures
Distance to stream	Dense networks = rapid flooding	Minimal	Not significant
Flow accumulation	Identifies main flood paths	Favors waterlogging in depressions	Not significant
Rainfall	Primary flood trigger	Recharge + evaporation → salinity	Triggers weathering & slope failures
Soil	Alluvial deposits prone to flooding	Sabkha = salt crusts; clayey soils retain water	Weak, expansive soils → slope failure
Soil salinity	Indirect (structural soil weakening)	Direct cause of soil/infrastructure degradation	Weakens sabkha ground stability
Soil moisture	High saturation reduces infiltration → runoff	Direct driver of shrink–swell, waterlogging	Reduces slope shear strength (Landslides)
Geology	Impermeable lithologies amplify runoff	Karst/evaporites → salinity & collapse	Rigid cliffs + fractured rocks prone to rockfall
LULC	Urban/bare = impervious → floods	Agriculture/irrigation increases salinity	Deforestation/urbanization destabilize slopes

Topography-based factors such as elevation and slope were reclassified using the Equal Interval method, while rainfall was categorized using the Quantile Interval method. Curvature was classified using the Natural Breaks method, classifying between negative values (convex), zero (flat), and positive values (concave). To ensure spatial consistency across datasets, all input raster layers were resampled to a uniform pixel resolution of 30 meters, aligning with the resolution of L9.

Geological features, such as basement complex rocks and Quaternary deposits, were clearly distinguishable using L9 Bands of 753 in RGB (Figure 6a and 6b). The classification into low, medium, and high susceptibility classes was based on spectral characteristics, field validation, and previous geological studies. Specifically, spectral differences in reflectance values in SWIR, NIR, and Red bands were used to differentiate rock types (Figure 6a). DEM gives elevation, slope, curvature, and drainage patterns, all of which influence geohazard susceptibility (Figure 6d). Soil classification, derived from FAO and UNESCO maps (Baillie, 2001; Hartemink et al. 2013). and refined using USDA soil taxonomy, revealed three main soil types: weathered basement soils, alluvial deposits, and recent coastal deposits (Figure 6d). Soil moisture, identified as a significant risk factor, can lead to structural settling (Figure 6e), while salinity, closely linked to soil moisture, was also critical; low land areas (Salalab, Al-Thawra, Hadal, Deim Alnoor, Korea, Flamingo) are highly susceptible to flash floods due to their tendency to accumulate water, intensified by poor drainage systems. These areas also contain shallow-depth groundwater, which contribute to higher soil moisture levels compared to the more stable and less permeable basement rocks in the west. This increased moisture preservation further influences geohazard susceptibility as a factor and criteria, impacting soil stability and infrastructure instability (Figure 7e).

LULC mapping highlighted bare ground and built-up areas as one class; flooded vegetation, trees and crops as class two and the water body as class three after reclassification (Figure 7f). Environmental factors, including rainfall (Figure 7a), humidity (Figure 7b), and temperature (Figure 7c), showed an eastward increase toward mountainous highlands and a decrease near coastal areas. Topographical factors, such as curvature (Figure 7d), slope (Figure 8d), and aspect (Figure 8e), were reclassified into three categories, with slope gradients ranging from level to steep areas, influencing runoff rates and mass movement across the study area. Hydrological factors, including drainage density, stream patterns, and flow accumulation, were reclassified and showed strong correlations with topographic features and geohazard susceptibility (Figure 8a–8c). Using AHP-derived weights, individual geohazard maps for each factor were generated, which were then integrated to produce a final geohazard susceptibility map, providing a comprehensive assessment of the study area.

4.3 Geohazard mapping

In the precent study, the applied AHP for geohazard susceptibility used an integration of different factors as mentioned above. Building on these factors, four main maps were obtained based on their contribution to hazard susceptibility (hydro-meteorological factors caused flash flood hazard, soil related factors (salinity and moisture) caused soil degradation hazard, topographic/terrain factor caused rock falling geohazard, geology with LULC related factor caused environmental hazards), with flood risk receiving the highest weight, followed by salinity, soil moisture, geology, and LULC. A pairwise comparison using a matrix to assess the relative importance of these factors (Tables 5 and 6).

For the topographical/terrain factors, the study area is characterized by strong, high-relief terrains, particularly in the western region. To account for this, significant weight (Equation 16) (Ali et al. 2019; Rashwan et al. 2024) was assigned to slope and curvature alongside other factors in generating a geohazard map (Figure 9). The results highlight the elevated areas of the Red Sea Hills as regions of high landslide risk, primarily due to steep slopes. However, in our specific study area, these high-risk zones remain largely uncovered by land development, modifying current hazards but highlighting the need for careful future planning.

$$Slope^{*}0.30 + Geology^{*}\ 0.20 + Drainage^{*}\ 0.15 + Rainfall^{*}\ 0.15 + LULC^{*}\ 0.10 + Soil^{*}\ 0.10 \quad (16)$$

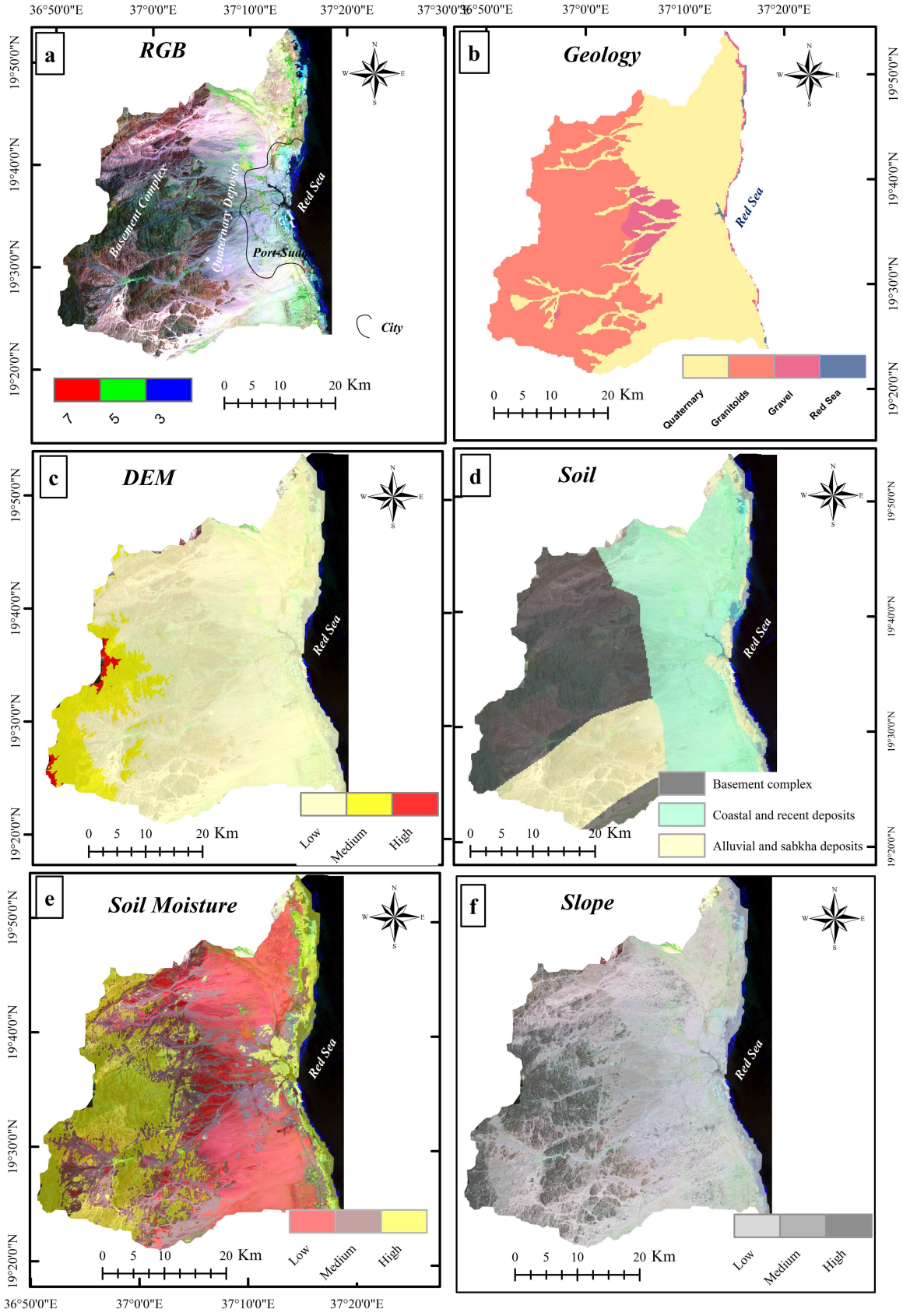

Figure 6. Classified geological factors; (a) L9 Bands of 753 in RGB; (b) classified geology; (c) DEM; (d) classified soil map; (e) soil moisture; (f) slope.

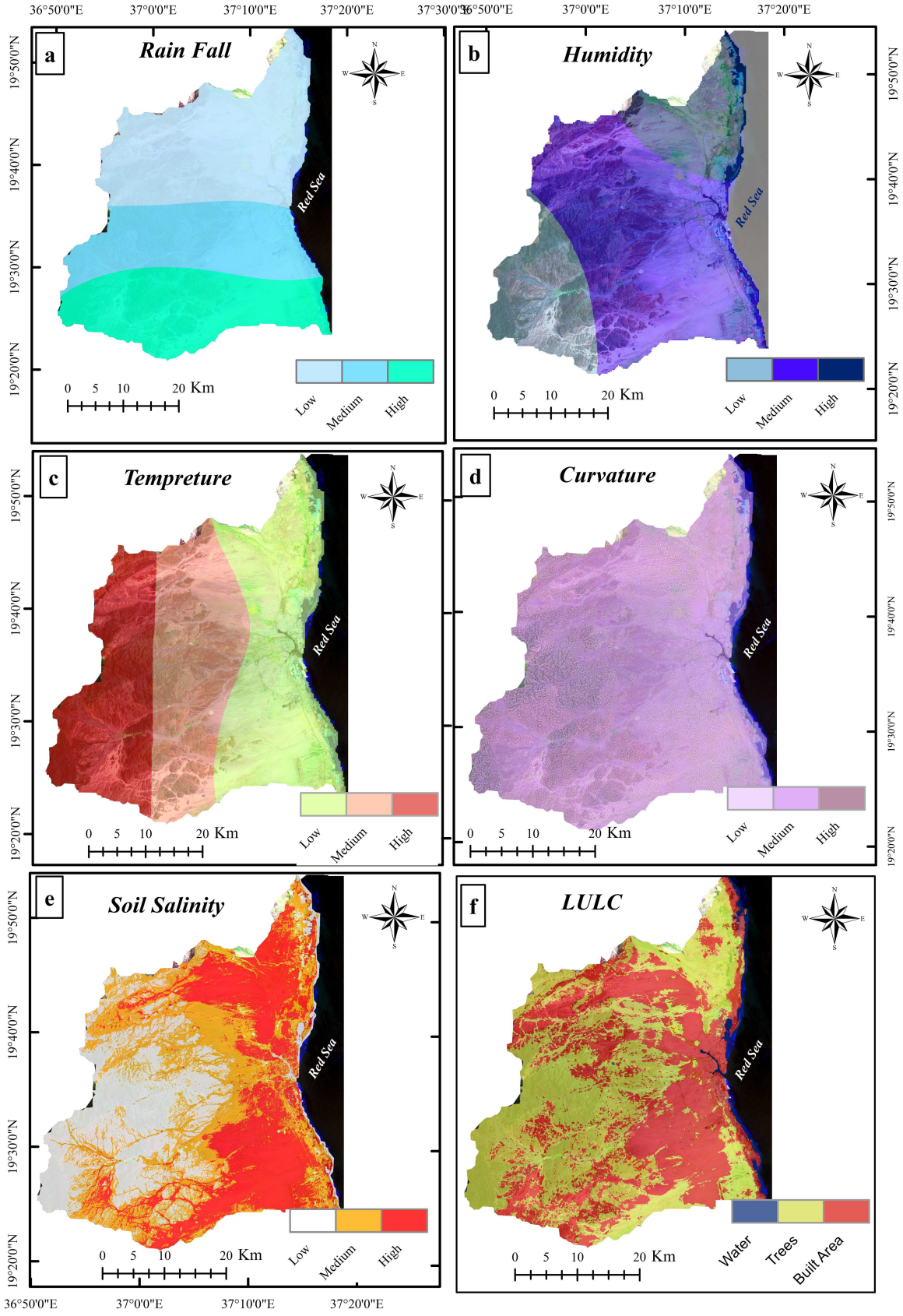

Figure 7. Classified environmental and human factors; (a) rainfall; (b) humidity; (c) temperature; (d) curvature; (e) soil salinity; (f) LULC map.

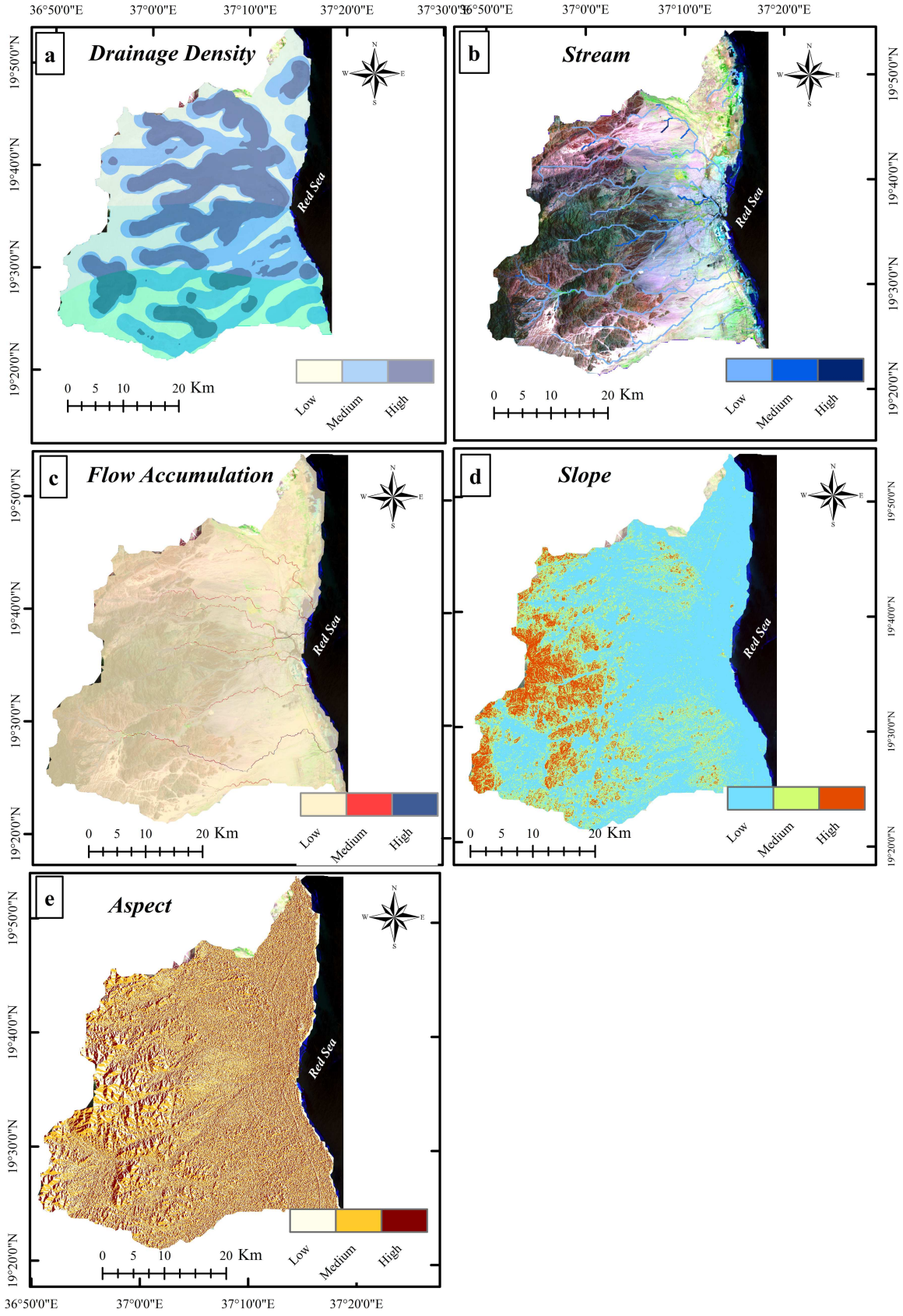

Figure 8. Classified hydrological factors of (a) distance to stream channels; (b) stream; (c) flow accumulation; (d) slope; (e) aspect map.

Table 5. Pairwise comparison matrix for factor criteria.

Factor	Elev.	Slope	Curvature	Geology	Soil	Salinity	Soil moisture	Distance to stream	Rainfall	Flow accumulation	Land cover
Elevation	1.00	1.00	0.50	3.00	3.00	0.50	0.50	4.00	4.00	4.00	1.00
Slope	2.00	2.00	1.00	2.00	2.00	1.00	1.00	2.00	2.00	2.00	2.00
Curvature	0.33	0.33	0.50	1.00	1.00	0.50	0.50	2.00	2.00	3.00	2.00
Geology	0.33	0.33	0.50	1.00	1.00	0.50	0.50	2.00	2.00	3.00	2.00
Soil	2.00	2.00	1.00	2.00	2.00	1.00	2.00	4.00	3.00	4.00	2.00
Salinity	2.00	2.00	1.00	2.00	2.00	0.50	1.00	1.00	2.00	1.00	2.00
Soil Moisture	0.25	0.25	0.50	0.50	0.50	0.25	1.00	1.00	2.00	2.00	0.33
Distance to stream	0.25	0.25	0.50	0.50	0.50	0.33	0.50	0.50	1.00	2.00	0.33
Rainfall	0.25	0.25	0.50	0.33	0.33	0.25	1.00	0.50	0.20	1.00	0.33
Flow Accumulation	1.00	1.00	0.50	0.50	0.50	0.50	0.50	3.00	3.00	3.00	1.00
Land cover	1.00	1.00	0.50	2.00	2.00	0.50	0.50	3.00	3.00	3.00	1.00
Total	**9.42**	**9.42**	**6.50**	**12.83**	**12.83**	**5.33**	**8.50**	**20.00**	**21.20**	**25.00**	**13.00**

Table 6. Percentage importance values using the analytic hierarchy process.

Factor	Dem	Slope	Curvature	Geology	Soil	Salinity	Soil moisture	Distance to stream	Rainfall	Flow accumulation	Land cover
Dem	0.096	0.096	0.071	0.189	0.189	0.086	0.056	0.167	0.157	0.138	0.071
Slope	0.096	0.096	0.071	0.189	0.189	0.086	0.056	0.167	0.157	0.138	0.071
Curvature	0.192	0.192	0.143	0.126	0.126	0.174	0.111	0.111	0.078	0.069	0.143
Geology	0.032	0.032	0.071	0.063	0.063	0.086	0.056	0.083	0.078	0.103	0.143
Soil	0.032	0.032	0.071	0.063	0.063	0.086	0.056	0.083	0.078	0.103	0.143
Salinity	0.192	0.192	0.143	0.126	0.126	0.174	0.222	0.078	0.118	0.138	0.143
Soil Moisture	0.192	0.192	0.143	0.126	0.126	0.174	0.222	0.078	0.078	0.034	0.143
Distance to stream	0.024	0.024	0.071	0.032	0.032	0.043	0.111	0.078	0.078	0.069	0.024
Rainfall	0.024	0.024	0.071	0.032	0.032	0.057	0.111	0.078	0.039	0.069	0.024
Flow Accumulation	0.024	0.024	0.071	0.021	0.021	0.043	0.111	0.020	0.118	0.103	0.024
Land cover	0.096	0.096	0.071	0.032	0.032	0.086	0.056	0.125	0.118	0.103	0.071
Total	1	1	1	1	1	1	1	1	1	1	1

Geology, soil and slope are the primary factors influencing geohazards in the study area (Equation (17)). A hazard susceptibility map (Figure 10) was generated, revealing that all areas near the Red Sea shoreline are classified as high-risk zones. This classification is primarily due to the intense moisture activity and high salinity levels associated with sabkha soils in the region. Additionally, moisture plays a critical role in hazard susceptibility, as evidenced by the high-risk classification of areas within major channels and khors, including Salalab, Mog, and Sallum. These findings are strongly supported by detailed field observations, which confirm the vulnerability of these zones to hazard results.

$$Geology * 0.20 + Slope * 0.20 + Drainage * 0.15 + Salinity * 0.15 + LULC * 0.10 + Soil * 0.10 \quad (17)$$

High salinity and moisture content can deal with soil stability by weakening its structure, increasing susceptibility to settling, compaction, and minor landslides, particularly on sloped terrains. In sabkha environments, subsidence may occur due to salt dissolution and cyclic volume changes from wetting and drying. Additionally, salt crystal growth within the soil can exert pressure, leading to cracking, which damages infrastructures. Salinity also reduces vegetation cover, exposing the soil to heightened erosion by wind and water. Collectively, these factors highlight the need for careful soil management to mitigate environmental and structural risks (Daliakopoulos et al. 2016; Ghazali et al. 2020; Sahab et al. 2021; Rengasamy et al. 2022; Maleki et al. 2024).

The susceptibility map of flash flood hazard derived from hydro-meteorological factors produced in this study highlights the southern part of the study area as the primary high-risk zone for flooding (Port Sudan International Airport and Bashair Liquids Storage Terminal and Port) (Figures 11 and 1c). This is attributed to factors such as high rainfall, steep slopes, and the lack of flood control structures, which result in significant flow accumulation and poor drainage (Equation (18)).

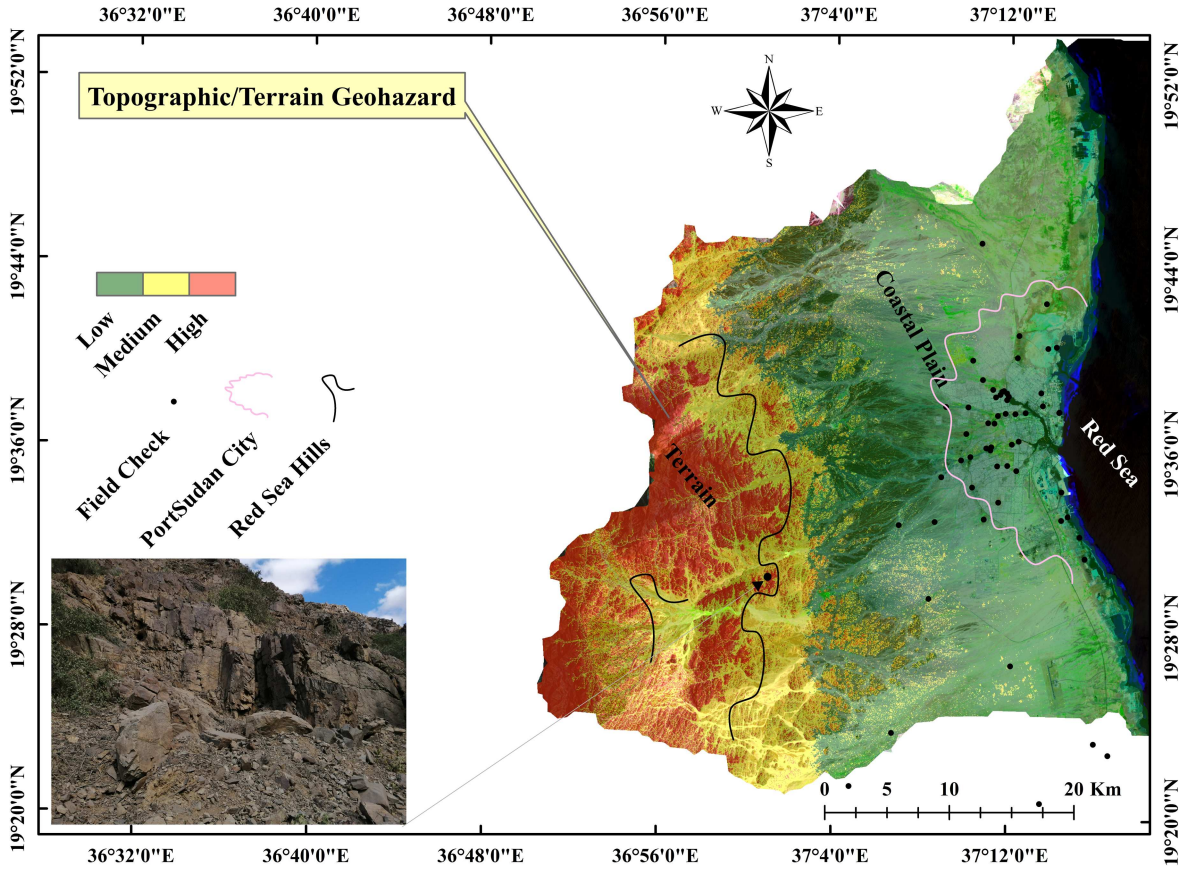

Figure 9. Terrain-based susceptibility map illustrating variations influenced by topographic features.

$$LULC * 0.20 + DEM * 0.20 + Geology * 0.15 + Rainfall * 0.14 + Drainage * 0.10 + Slope * 0.10 + Soil0.06 + Salinity * 0.10 \quad (18)$$

The weights assigned to rainfall, flow accumulation, and drainage density reflect their strong influence on flood susceptibility, with field observations and historical data supporting these findings. However, the current evaluation does not account for recent changes in the northern part of the study area, particularly the collapse of the Arbaat Dam due to high flow accumulation and silting up in August 2024. The northern part, which previously benefited from the flood regulation capacity of the Arbaat Dam, is now expected to face increased flood risks during the next rainfall seasons. These changes are likely to shift the dynamics of flood susceptibility, with the northern part becoming more vulnerable than the southern part (Figure 12).

After analyzing and testing individual hazard susceptibility maps for each contributing factor following different methods suggested by different researchers over the word (Mason and Rosenbaum 2002; Vaziri et al. 2018; Obiegbu 2021), we developed a final integrated geohazard map (Figure 13) corresponding to the main factors according to (19). The final map highlights areas with varying degrees of susceptibility, presenting a clear and actionable visualization of geohazard risks in the study area (Figure 9).

$$DEM*22.5 + Slope* 22.5 + Curvature* 16.5 + Geology* 12.5 + Soil*12.5 + Salinity*25 + Moisture* 16.5 + Drainage*7.25 + Rainfall*7.75 + Flow\ accumulation*7.75 + LULC15.25 \quad (19)$$

This geohazard mapping approach underscores the importance of multifactorial assessments in geohazard studies. Using the AHP, we systematically integrated different datasets, while field observations validated the findings, ensuring accuracy and reliability. The results demonstrate the effectiveness of this

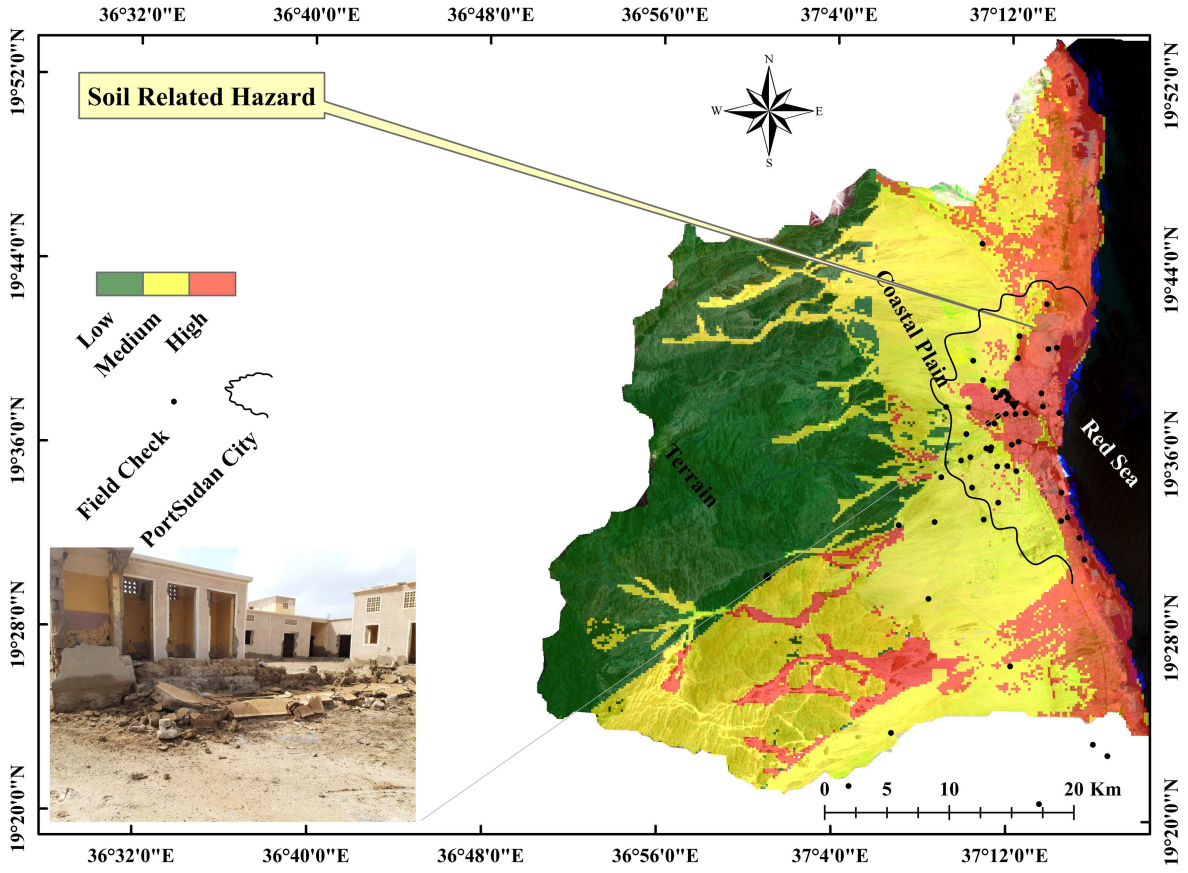

Figure 10. Geohazard map of Port Sudan City derived from geology and soil factors, highlighting areas where buildings are highly susceptible to collapse.

method in addressing geohazard challenges and provide a replicable framework applicable to similar environments worldwide.

Notably, the destructive effects of soil salinity and excessive moisture on infrastructure in the study area are apparent from field surveys and laboratory analyzes. Buildings in high-salinity zones, particularly those on sabkha soils, exhibit significant structural damage, including foundation erosion, wall cracking, and irregular settlement, all of which compromise structural stability.

The final geohazard map aligns well with the field validated checkpoints; however, some misclassifications were observed. These differences may be attributed to the weighting significance in the overlay process, as each factor such as flooding zones, salinity effects, and topographical influences contributes differently to the overall hazard assessment. In some cases, specified points fall within multiple hazard categories or in low-risk zones, making classification more complex. Despite these minor variations, the integrated approach remains a strong tool for geohazard evaluation, providing effective understandings for risk assessment and improvement development.

4.4 Validation

A pairwise comparison was carried out using the AHP to assess the relative importance of the eleven conditioning factors for multi-hazard susceptibility mapping (Table 5). The comparison matrix reflects expert-based judgments, field observations, and insights from previous studies in similar environments. The diagonal values equal 1, while off-diagonal entries express how much more one factor influences hazard occurrence relative to another. For example, slope, soil, and geology were judged more influential than curvature and rainfall, reflecting their dominant role in runoff concentration, infiltration, and geomorphological control.

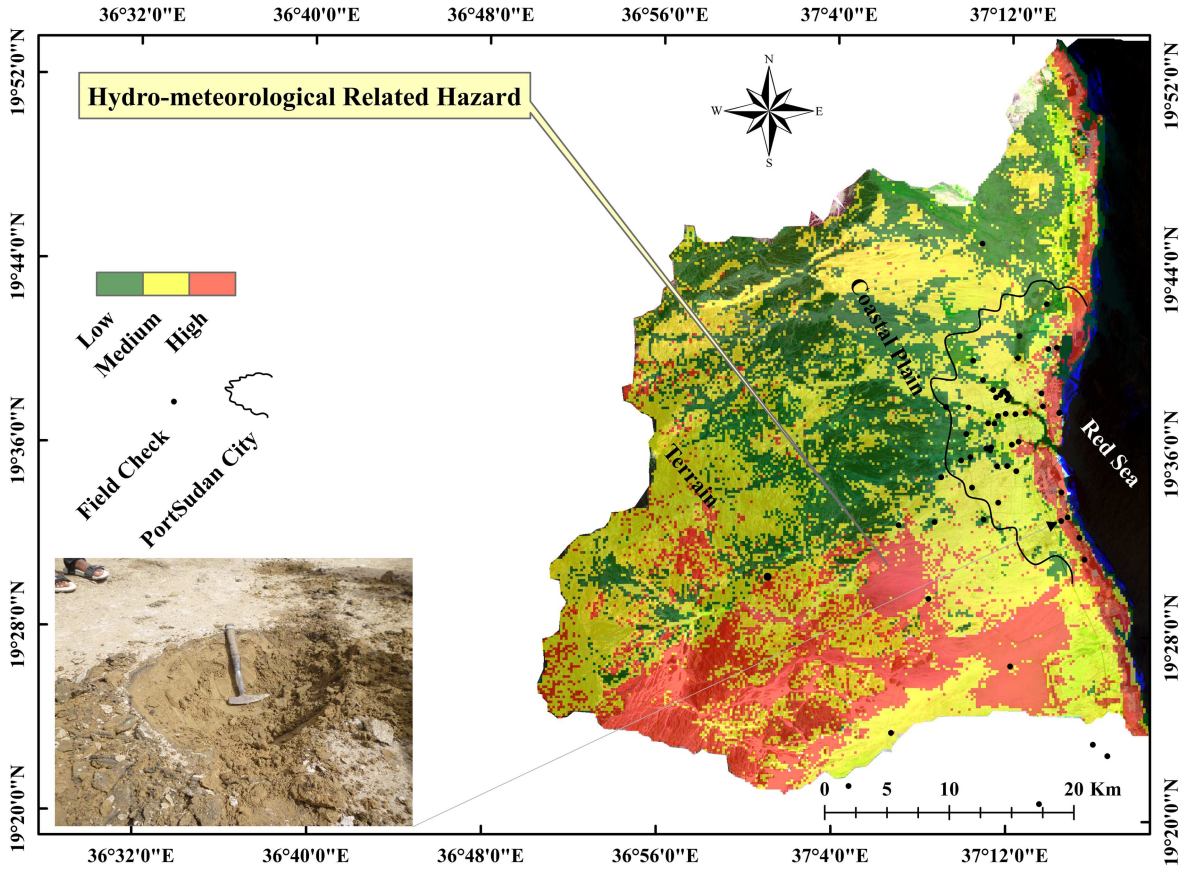

Figure 11. Hydro-meteorological related factors susceptibility map of the Port Sudan City.

Table 6 shows the normalized weights derived from the comparison matrix. These weights represent the final contribution of each factor to hazard susceptibility. The results indicate that drainage density (0.167), rainfall (0.157), and flow accumulation (0.138) were the most influential hydrological factors. Among terrain-related factors, slope (0.096) and elevation (0.096) carried notable weights, highlighting their importance in flash flood initiation. Soil-related factors such as salinity (0.174) and soil moisture (0.174–0.222 in some comparisons) also received significant influence, underlining their role in land degradation and secondary hazards.

To evaluate the robustness of the MCDA framework, a sensitivity analysis was performed to examine how variations in factor weights influence the final hazard susceptibility outcomes. The sensitivity statistics (Table 7) include the minimum, maximum, mean, and standard deviation of changes in susceptibility scores when factor weights were systematically adjusted.

The results demonstrate that some factors exert a stronger influence on the model output than others. Geology related factors showed the highest variability, with a wide range (−12.95 to 14.37), indicating that lithological conditions are a critical determinant of hazard susceptibility in the study area. Topographic/terrain related factors also exhibited strong sensitivity (means of −3.46 and −4.15, respectively), underscoring their importance in controlling runoff, erosion, and flash flood potential.

On the other hand, Hydro-meteorological factors such as flow accumulation (mean −3.25) and rainfall (mean −2.50) contributed moderate sensitivity, reflecting their direct role in hydrological processes. Soil related factors, LULC, and distance to stream showed lower standard deviations, suggesting that their influence on the final hazard zonation is more stable and less sensitive to weight adjustments.

Interestingly, soil moisture and salinity demonstrated relatively small ranges compared to geological and topographic factors. This indicates that while they are significant for localized hazards (e.g. waterlogging, soil degradation), their overall impact on susceptibility mapping is less variable.

Field surveys were conducted across many sections of the study area to assess and validate hazard classifications, specifically identifying regions of high, medium, and low risk based on the type of hazard

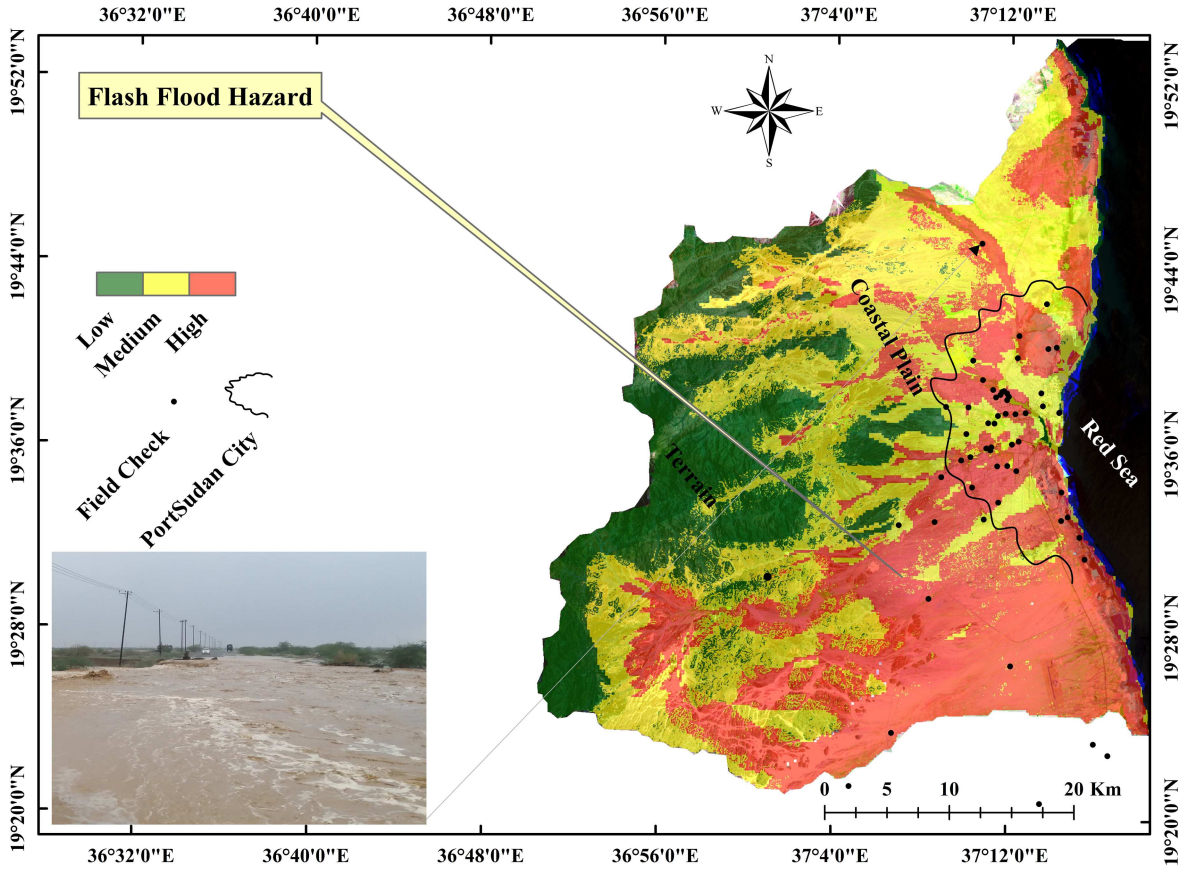

Figure 12. Flash Flood Susceptibility Map of Port Sudan City showing the spatial distribution of risk zones based on the AHP model.

present. A total of 30 locations were visited to evaluate flash flood areas, including key Khors such as Arbaat, Salalab, Mog, Kilab, Korea, and Salum. Other field trips were conducted to reveal the destructive effects of soil salinity and excessive moisture on infrastructure in the study area. Buildings exhibit significant structural collapse, particularly in areas with high salinity levels (Figure 14).

Laboratory tests were conducted on representative soil samples collected from the study area to evaluate their geotechnical characteristics (Table 8). The measured moisture content values ranged from 1.64% to 15.87%, indicating variable water retention across the sites. Higher moisture contents were generally associated with low-lying areas and poorly drained locations, while elevated and well-drained sites exhibited lower values.

The grain size distribution (sieve analysis) showed that a significant proportion of the soil passed through the No. 200 sieve, ranging between 71.2% and 97.2%, confirming the dominance of fine-grained materials. This suggests that the soils are generally prone to reduced permeability and potential for waterlogging. The fraction passing the No. 40 sieve was even higher (84–99.4%), further supporting the fine-textured nature of the soils.

The Atterberg limits indicated moderate plasticity, with liquid limits (LL) between 24.0 and 30.4 and plastic limits (PL) ranging from 18.1 to 20.8. The calculated plasticity indices highlight the soil's tendency to exhibit some cohesion but remain predominantly silty in behavior.

5 Discussion

The city of Port Sudan, located on the coast of the Red Sea, as the main port of the country, is also crucial from a strategic point of view and from the point of view of international trade. However, its position between the Red Sea Hills and the Red Sea makes it extremely vulnerable to geohazards. Seasonal water

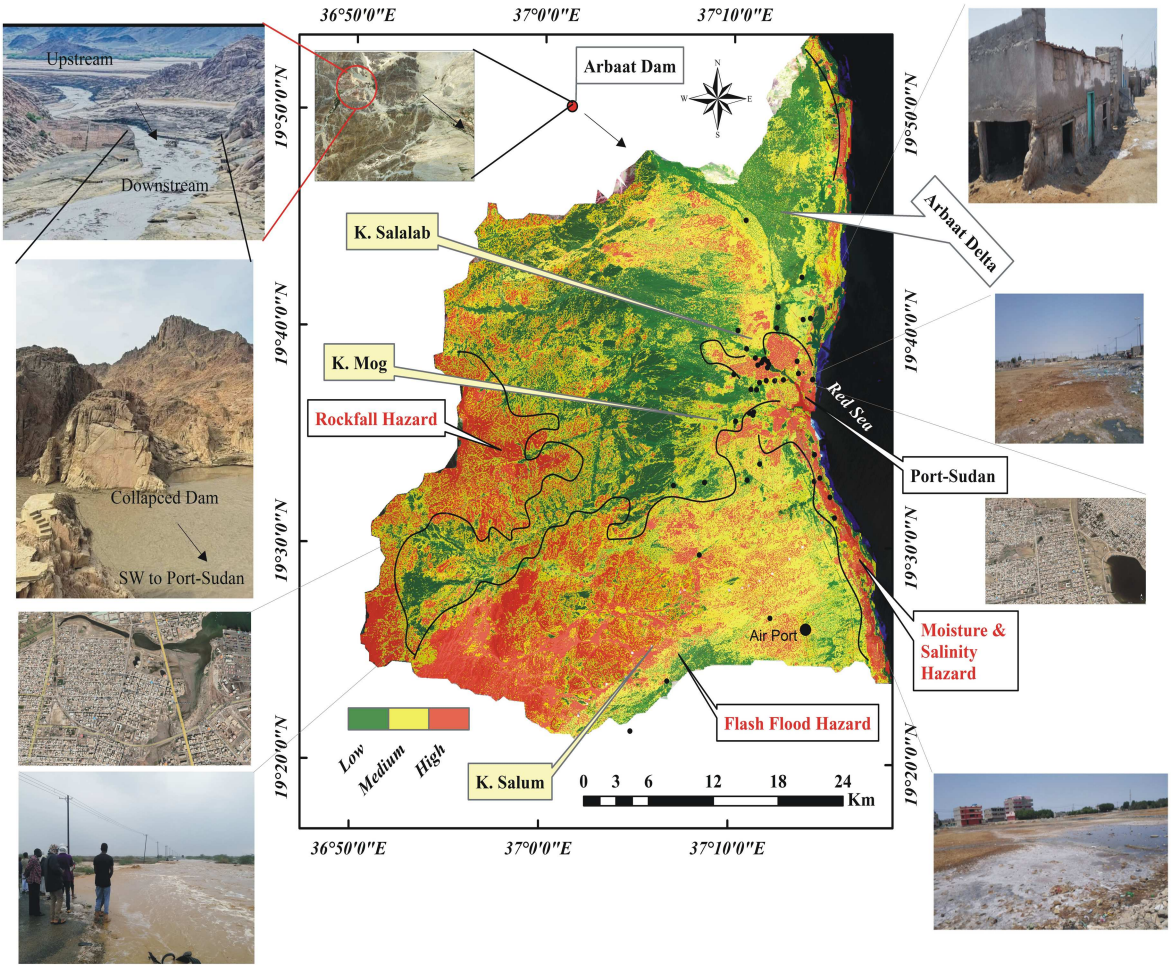

Figure 13. Final synthesized geohazard susceptibility map of Port Sudan City based on all contributing factors.

Table 7. Sensitivity results of each factor.

Factor sensitivity	min	max	mean	Stander deviation
Soil moisture	−8.97	2.4	−1.9	2.28
Geology and lithology	−12.95	14.37	−2.91	1.6
Slope	−9.28	1.58	−3.46	1.51
Salinity	−5.75	1.21	−2.14	1.37
Curvature	−7.7	1.18	−2.28	1.11
Elevation	−9.37	1.12	-4.15	1
Soil type	−5.8	0.3	−2.49	0.98
LULC	−693	1.26	−1.46	0.91
Distance to stream	−5.65	−0.4	−2.41	0.76
Rainfall	−6.13	−0.45	−2.5	0.64
Flow accumulation	−6.13	−0.97	−3.25	0.43

flows from the surrounding basement terrains towards the coast frequently resulting in floods, soil salinity, and soil moisture concerns. These natural hazards are combined with human activities, including artisanal mining and soil excavation along flood channels, destabilizing the landscape, increasing flood risks, and degrading the environment. The lack of a comprehensive geohazard strategy establishes significant risks to the city's infrastructure, public health, and ecosystems. Effective geohazard mapping is crucial for mitigating these risks. Comprehensive geohazard assessments can improve disaster awareness and adaptability by integrating environmental, hydrological, and geological factors (Sandoval et al. 2023; Huang et al. 2023).

The study represents the first attempt to develop a comprehensive geohazard susceptibility map for the study area by integrating multidisciplinary data using the MCDA and AHP. Through this approach, we aimed to address the critical need for effective risk management and sustainable land-use planning. The

Figure 14. Field observation and validation showing; (a) salinity and moisture effect on buildings; (b) collapse due to rising of salinity and moisture; (c) flash flood event during the field survey; and (d) sabkha soil in different parts of the study area.

Table 8. Summary of laboratory test results of soil samples from different parts of the study area.

Sample	Locality	MC (%)	CU	CC	LL (%)	PL (%)	PI	PH	Sulfate (ppm)	Chloride (ppm)	Salt content	Type
S1	*Hai-Khalij*	15.87	3.33	0.40	24.0	19.76	4.24	9.92	0.7	0.22	Low	Sabkha soils
S2	*Falamingo*	2.12	5.00	0.45	25.1	18.10	7.0	8.92	1.17	1.59	High	
S3	*Salalab1*	8.35	3.00	0.83	24.8	20.80	4.0	8.74	0.9	3.9	High	
S4	*Kilo*	6.23	2.14	0.77	30.39	20.85	9.54	9.15	0.9	2.5	High	
S5	*Salalab 2*	14.88	4.8	0.6	36.54	66.0	30.96	10.2	1.9	2.16	Very High	
S6	*HaiAlmatar*	2.83	10	6.4	29.0	19.7	10.7	8.14	0.5	0.12	Low	
S7	*Walli*	1.64	7.69	0.7	31	21.25	9.75	8.73	1.1	1.4	High	
S8	*Sallum*	10.71	3.85	0.7	30.47	54.80	24.33	9.97	1.7	1.3	Very high	
S9	*Center*	1.5	3.75	0.03	54.8	30.47	24.44	7.91	–	–	–	Marl (coral reef
S10	*Soug*	0.91	4.92	1.0	66	36.54	30.93	8.42	–	–	–	limestone)
S11	*Korea*	6.6	2.48	0.41	–	NP	NP	–	–	–	–	Gravely sand (older
S12	*Ring road1*	D	55.14	1.11	41.32	27.25	14.7	–	–	–	–	gravels)
S13	*K. Mog*	D	32.48	0.53	–	NP	NP	–	–	–	–	
S14	*K. Salalab*	D	42.22	1.0	40	23.33	16.67	–	–	–	–	
S15	*Bashaer1*	1.82	7.8	0.63	–	NP	NP	–	–	–	–	Quaternary deposits
S16	*Bashaer2*	8.40	40	1.44	48	24.02	23.98	–	–	–	–	
S17	*Bashaer3*	5.6	25	0.67	59	22.65	36.35	9.80	0.9	0.23	Low	
S18	*Shoreline1*	21.29	–	–	36	21	15	10.2	2.4	4.3	Very High	Sabkha soils
S19	*Shoreline2*	10.88	–	–	36	20	16	9.21	1.8	2.5	Very High	
S20	*Shoreline3*	12.97	–	–	38	15	23	11.3	2.2	2.34	Very High	
S21	*Hadal*	19.2	–	–	39	26	13	9.0	0.7	2.4	High	
S22	*Arbaat*	D	55.14	1.11	54.8	30.47	24.33	–	–	–	–	Quaternary deposits

MC: Moisture content, LL: Liquid limit, PL: Plastic limit, PI: Plasticity Index, CU: Uniformity coefficient, CC: Coefficient of curvature, NP: Non plastic, D: dry.

weighting of the selected factors (hydro-meteorological, soil, geology, and LULC) was determined based on their relative significance in influencing geohazards. Flood risk was assigned the highest weight (1), reflecting its substantial impact on the study area, particularly due to seasonal water flows and human-induced alterations along flood channels; salinity (2) and soil moisture (3) were highlighted due to their effect on soil degradation and potential impacts on infrastructure stability; geology (4) and LULC (5) further contributed to recognizing the broader environmental and land-use dynamics that intensify geohazards (Figures 9 and 10).

Using these weights, we developed four geohazard maps corresponding to each of the main factors and an integrated geohazard susceptibility map that produces these individual layers. The integrated map highlights areas with varying degrees of susceptibility, providing a clear and actionable visualization of geohazard risks in the study area.

This geohazard mapping approach underscores the importance of multifactorial assessments in geohazard studies. The use of AHP allowed for the systematic integration of different datasets, while field and laboratory observations validated the findings, ensuring accuracy and reliability. The results demonstrate the utility of this method for addressing geohazard challenges, advancing a replicable framework that could be applied in similar environments globally.

The destructive effects of soil salinity and excessive moisture on infrastructure in the study area are evident from field surveys and laboratory analyzes. Buildings in high-salinity areas (Sabkha soil) show significant structural damage, such as foundation erosion, wall cracking, and irregular settlement, all of which settlement structural stability. The chemical degradation caused by high concentrations of sulfates and chlorides in sabkha soils is particularly concerning. These salts corrode both concrete and steel, indicating material weakening and increased vulnerability to collapse.

Sabkha soils, commonly found along the Red Sea coast and arid regions of Sudan, are characterized by their high salinity, low bearing capacity, and susceptibility to flooding (Arifuzzaman et al. 2016; Rajendran et al. 2021; Aloui et al. 2024; Wahba et al. 2024). These soils are formed in environments with low wave energy, where fine sediments such as silt and clay are loosely cemented by evaporative salts (Erol 1989; Griffiths et al. 2012). This complex formation process results in high void ratios and compressibility, which lead to substantial consolidation and settlement when structures are built on them.

Geohazard mapping conducted in the study identified 14 high-risk zones for construction, including Alsouq-Alshaabi, Salalab Block 6, and South Port Damadama, where excessive salinity and moisture are most evident (Figure 10). Notably, the Salalab area, situated within the Khor of Salalab, is significantly affected by water flow and sediment transport from the western Red Sea Hills, increasing both flood and salinity risks. Soil salinity and moisture maps validated by field surveys confirmed the destructive effect on infrastructure, such as foundation erosion, wall cracks, and settlement. The geohazard map underscores the urgent need for designed engineering solutions to mitigate these risks. Proposed strategies include soil stabilization through chemical methods like lime or cement treatment to enhance load-bearing capacity, improved drainage systems to minimize flooding and capillary rise, the use of protective coatings for corrosion resistance, and flood mitigation measures such as levees and barriers to safeguard against flash floods. These involvements are essential for mitigating the complex geotechnical and environmental experiments caused by sabkha soils in the region (Figures 10, 13 and 14).

While the current susceptibility map of flash flood highlights the southern part as the primary high-risk zone, it does not account for the recent collapse of the Arbaat Dam (Hamid 2022; Ahmed 2024; Sulieman et al. 2024). This event has fundamentally altered hydrological dynamics in the northern sector, eliminating the dam's regulatory capacity and thereby increasing the likelihood of severe flooding in areas previously considered relatively safe. As a result, the existing map should be interpreted with caution, as it underrepresents the newly emerging risks in the northern part of the city.

The Arbaat Dam collapse underscores the dynamic and evolving nature of hazards in the study area. Although the present results classify the southern sector as the most flood-prone, the northern part is now expected to face substantially heightened risks in upcoming rainy seasons. To address this shift, three immediate actions are recommended: (i) updating susceptibility mapping using post-collapse satellite imagery and hydrological datasets, (ii) initiating hydrodynamic modeling and field surveys to represent altered flow pathways, and (iii) strengthening infrastructure resilience and community preparedness to mitigate impacts on vulnerable populations and critical facilities.

Despite this limitation, the susceptibility analysis remains valuable in identifying the most influential hazard factors across the entire city namely hydro-meteorological factors, soil related factors, and terrain related factors, while rainfall intensity, elevation, aspect, slope, and land use were less influential. Accordingly, the study area was classified into three zones of hazard probability: high, medium, and low. Together with recognition of the Arbaat Dam collapse, these results provide an updated foundation for risk-informed planning and adaptive land-use strategies in Port Sudan.

The validation of susceptibility mapping was approached through multiple complementary methods. Field observations and photographic evidence of past flood traces confirmed that high-hazard zones in the model correspond closely with the locations that experienced severe flooding, thus providing direct ground-truth validation. Laboratory analyzes of soil samples, including moisture content, sieve tests, and Atterberg limits, further reinforced the findings by showing that the soils in high-susceptibility areas are predominantly silty sands with relatively low cohesion and moderate to high moisture retention capacity, conditions that enhance runoff and reduce infiltration. In addition, the sensitivity analysis reveals good overview of each factor's contribution towards the risk potential value of each cell or region; the statistical results of this analysis are provided in Table 7.

From analysis, it is clear to extract that the geohazard generated map is mainly effective to five factors: soil moisture, geology and lithology, slope, salinity and curvature according to the highest value of the standard deviations of the calculated sensitivity index (SI), where the lowest effective factors are elevation, soil type, LULC, drainage density, rainfall and flow accumulation. However, this doesn't mean the model is not sensitive to the lowest effective factors or to the other factors, as the mean values of the potential areas are relatively in the same range. Field surveys and checkpoints confirm that moisture is a major contributor to infrastructure and ecosystem damage. The overlay of the validations with the susceptibility maps shows strong agreement, with more than four–fifths of recorded flood traces located within the mapped high hazard classes. This alignment provides direct, empirical confirmation that the AHP-derived weights and factor selection were appropriate for the study area.

Although this study provides a comprehensive geohazard assessment for Port Sudan City, several limitations remain and opportunities for future research are evident. The study area is still largely unexplored in terms of detailed geohazard mapping, highlighting the need for high-resolution investigations into soil salinity and moisture distribution, particularly considering seawater intrusion and the interactions between saline, brackish, and fresh groundwater. Understanding these water–rock–soil interactions is critical for accurately modeling geohazard susceptibility.

In addition, detailed geotechnical studies of saline soils, including borehole sampling of sabkha areas, are necessary to evaluate soil strength, compressibility, and stability under varying moisture and salinity conditions. Such investigations would provide essential data for infrastructure planning and hazard mitigation. The recent collapse of the Arbaat Dam in the northwestern part of the study area further underscores the importance of updating geohazard maps, as this event has significantly altered flood dynamics and risk distribution.

While the current AHP-GIS framework provided reliable susceptibility maps supported by field/lab observations, incorporating advanced machine learning and deep learning approaches (e.g. RF, XGB, SVM, KNN, CNN, etc.) in future research could enhance predictive accuracy of susceptibility mapping of flash flood, rock falling, and landslides (Kainthura and Sharma 2022; Liu et al. 2023; Elomiya et al. 2024; Yaghoubi et al. 2024; Lokesh et al. 2025), and better capture complex spatial relationships among environmental, hydrological, and geological factors. Finally, continuous updates to geohazard maps and their integration into urban planning, infrastructure development, and land-use management are essential to mitigate risks and support sustainable development in Port Sudan City.

6 Conclusions

The integrated hazard susceptibility map is complete as a critical tool for guiding decision-makers in mitigating risks, planning urban expansion, and stimulating sustainable land management. The current study underscores the urgent need to balance environmental protection with urban growth, particularly in areas like Port Sudan, where rapid population growth and economic activities have considerably heightened vulnerability to natural hazards due to its environmental and geological conditions; as a consequence,

the area faces to increasingly geohazard challenges. The city's high humidity accelerates infrastructure deterioration, while geological hazards such as floods, landslides, and subsidence establish substantial risks. Despite these risks, there remains a notable lack of geological studies to inform urban planning, highlighting the need for more comprehensive research and protection strategies.

Through this research, modern techniques such as GIS and remote sensing base MCDA and AHP were employed to produce a preliminary hazard risk map, for the first time in Port Sudan region. Using GIS and the AHP, areas with very high risk, including local districts such as (Salalab and Deim Al-Noor) were identified. These regions are particularly susceptible to environmental and geological factors, such as flooding, soil salinity, and structural instability. The map provides a foundation for current protective evaluations, such as constructing dams to relieve flood risks, improving drainage systems, and avoiding construction on saline soils. This study also emphasizes the importance of soil analysis to assess its geological and engineering properties before development, particularly in areas like Al-Thawra and Salalab, where saline soils threaten stability infrastructure. The research highlights the potential for expanding geohazard assessments to address other risks, such as desert encroachment, sand dunes, and rockfalls along critical routes like the New and Old Aqaba Road.

This establishing effort shows a suggestion to leverage geosciences to address the environmental and natural disagreements challenging the city. Moving forward, the research underscores the necessity of interdisciplinary collaboration among earth sciences, engineering, and environmental fields to develop comprehensive solutions. By integrating detailed fieldwork, geophysical studies, and advanced risk mapping, these efforts can ensure safety, reduce vulnerabilities, and contribute to sustainable development in the region.

Within the framework of this research, a preliminary geohazard risk map has been produced, considered the first of its type in the Port Sudan area. This research proudly stands out as a pioneer in the field of geological risk analysis, applying an innovative methodology to create this map. Future work could build on this study by exploring how climate change, sea-level rise, and continued urban expansion may affect geohazard levels in Port Sudan. Further studies could also apply advanced modeling techniques, long-term monitoring of soil salinity and moisture, and more detailed geological and geotechnical investigations. These efforts would help improve hazard prediction, strengthen planning strategies, and provide a clearer understanding of how risks may evolve in the coming years.

Acknowledgements

The authors thank the USGS, NASA–METI/ERSDAC, and LP DAAC for essential satellite imagery and geospatial data; the FAO for soil maps; the CRU for rainfall and flooding datasets; and the HydroSHEDS initiative for watershed data. Their contributions were instrumental to the successful completion of this research. The authors also acknowledge the financial and institutional support provided by the University of Debrecen Program for Scientific Publication.

Disclosure statement

The authors declare there is no conflict of interest in the preparation of this study. All research activities, including data collection, analysis, and interpretation, were conducted independently, and no external parties influenced the outcomes or conclusions of this work.

Data availability statement

The data sets used and/or analyzed during the current study are available from the corresponding author upon request.

References

Abdelkader M, Csámer A. 2025. Comparative assessment of machine learning models for landslide susceptibility mapping: a focus on validation and accuracy. Nat Hazards. 121(9):10299–10321. https://doi.org/10.1007/s11069-025-07197-0

Abubakar F, Abir I, Hassan A. 2025. Kogi west geophysical mineralisation appraisal using Analytical Hierarchy Process (AHP). J Afr Earth Sci. 224:105532. https://doi.org/10.1016/j.jafrearsci.2024.105532

Abu-Fatima M, Marignac C, Cathelineau M, Boiron M. 2021. Metallogeny of a Pan-African oceanic arc: VHMS and gold deposits in the Ariab-Arbaat belt, Haya terrane, Red Sea Hills (Sudan). GondR. 98:76–106. https://doi.org/10.1016/j.gr.2021.06.001

Agogue Feujio D, Aretouyap Z, Tchato S, Ngog II Legrand C, Djomdi E, Nague Madadjeu N, Nguimfack Nguimgo C, Ndinchout Kpoumie A. 2024. Application of analytical hierarchy process to assess groundwater potential for a sustainable management in the Menoua division. Heliyon. 10(2):e24310. https://doi.org/10.1016/j.heliyon.2024.e24310

Ahmad I, Farooq R, Ashraf M, Waseem M, Shangguan D. 2025. Improving flood hazard susceptibility assessment by integrating hydrodynamic modeling with remote sensing and ensemble machine learning. Nat Hazards. 121(7):7839–7868. https://doi.org/10.1007/s11069-025-07109-2

Ahmed M. 2024. Impacts of dams construction and water harvesting programs on community perception Red Sea in eastern Sudan. Sci Res. 13(2):21–31. https://doi.org/10.2139/ssrn.4862238

Ahmed A, Argaz A, Ouahman B, Darkaoui A, Bikhtar H, Ayouch E, Lazaar R. 2019. J Mater Environ Sci. 10(2):170–181. http://www.jmaterenvironsci.com. Flood Hazard Mapping Using remote sensing and GIS Tools: a case study of Souss Watershed Water ressources in Souss river basin View project Flood Hazard Mapping Using remote sensing and GIS Tools: a case study of Souss Watershed.

Akinlalu A, Afolabi D, Sanusi S. 2024. Knowledge-driven fuzzy AHP model for orogenic gold prospecting in a typical schist belt environment: a mineral system approach. ESE. 8(2):221–263. https://doi.org/10.1007/s41748-024-00382-4

Akter T, Hoque M, Mukul S, Pradhan B. 2025. Coastal flood induced salinity intrusion risk assessment using a spatial multi-criteria approach in the South-Western Bangladesh. ESE. 9(1):31–49. https://doi.org/10.1007/s41748-024-00399-9

Ali S, Biermanns P, Haider R, Reicherter K. 2019. Landslide susceptibility mapping by using a geographic information system (GIS) along the China–Pakistan economic corridor (Karakoram Highway), Pakistan. Nat Hazards Earth Syst Sci [Internet]. 19(5):999–1022. https://doi.org/10.5194/nhess-19-999-2019

Allafta H, Opp C, Patra S. 2021. Identification of groundwater potential zones using remote sensing and GIS techniques: a case study of the shatt Al-Arab Basin. Remote Sens (Basel). 13(1):1–28. https://doi.org/10.3390/rs13010112

Aloui S, Zghibi A, Mazzoni A, Elomri A, Al-Ansari T. 2024. Identifying suitable zones for integrated aquifer recharge and flood control in arid Qatar using GIS-based multi-criteria decision-making. Groundw Sustain Dev. 25:101137. https://doi.org/10.1016/j.gsd.2024.101137

Arabameri A, Pal S, Rezaie F, Nalivan O, Chowdhuri I, Saha A, Lee S, Moayedi H. 2021. Modeling groundwater potential using novel GIS-based machine-learning ensemble techniques. J Hydrol Reg Stud. 36(June):100848. https://doi.org/10.1016/j.ejrh.2021.100848

Arifuzzaman M, Habib M, Al-Turki M, Khan M, Ali M. 2016. Improvement and characterization of sabkha soil of Saudi Arabia: a review. J Teknol. 78(6):1–11. https://doi.org/10.11113/jt.v78.5352

Ashfaq S, Tufail M, Niaz A, Muhammad S, Alzahrani H, Tariq A. 2025. Flood susceptibility assessment and mapping using GIS-based analytical hierarchy process and frequency ratio models. Glob Planet Change. 251:104831. https://doi.org/10.1016/j.gloplacha.2025.104831

Avdan U, Jovanovska G. 2016. Algorithm for automated mapping of land surface temperature using LANDSAT 8 satellite data. J Sens. 2016:1–8. https://doi.org/10.1155/2016/1480307

Babikir I, Nagm E, Bamousa A, Barazi N. 2021. Facies analysis of the quaternary fluvial system of Khor Eit, Red Sea coast, Sudan. JAfES. 184:104370. https://doi.org/10.1016/j.jafrearsci.2021.104370

Badavath N, Sahoo S. 2025. Geospatial assessment and integrated multi-model approach for landslide susceptibility mapping in Meghalaya, India. AdSpR. 75(3):2764–2791. https://doi.org/10.1016/j.asr.2024.11.052

Barman J, Biswas B, Rao K. 2024. A hybrid integration of analytical hierarchy process (AHP) and the multiobjective optimization on the basis of ratio analysis (MOORA) for landslide susceptibility zonation of Aizawl, India. Nat Hazards. 120(9):8571–8596. https://doi.org/10.1007/s11069-024-06538-9

Beck H, Zimmermann N, McVicar T, Vergopolan N, Berg A, Wood E. 2018. Present and future Köppen-Geiger climate classification maps at 1-km resolution. Sci Data. 5(1):180214. https://doi.org/10.1038/sdata.2018.214

Becker M. 2006. Potential for satellite remote sensing of ground water. Ground Water. 44(2):306–318. https://doi.org/10.1111/j.1745-6584.2005.00123.x

Bedada B, Dibaba W. 2025. Geoinformatics and AHP multi criteria decision making integrated flood hazard zone mapping over Modjo catchment, Awash river basin, central Ethiopia. Discov Appl Sci. 7(4):284. https://doi.org/10.1007/s42452-025-06647-5

Bosworth W. 2015. Geological evolution of the Red Sea: historical background, review, and synthesis. In: Rasul, Stewart I. (eds) The Red Sea. Springer. p 45–78. https://doi.org/10.1007/978-3-662-45201-1_3.

Brakman S, Kohl T, van Marrewijk C. 2025. World population and trade in the 21st century. Rev Int Econ. 33(2):486–501. https://doi.org/10.1111/roie.12782

Baillie, IC. 2001. A basic system of soil classification for making and interpreting soil surveys. In: Soil Survey Staff 1999, Soil Taxonomy. Agricultural Handbook. Nat Resour Conserv Serv p 57–60. https://doi.org/10.1111/j.1475-2743.2001.tb00008.x.

Cangiano A. 2024) The future of population data.United Nations Population FundUniversity of Oxford https://ora.ox.ac.uk/objects/uuid:fa76de99-ec35-41ae-b6d6-1d9efb5791d8

Chelariu O, Minea I, Iațu C. 2024. Integrated assessment of geophysical and social vulnerability to natural hazards in North-East Region, Romania. Geomat, Nat Hazards & Risk. 15(1). https://doi.org/10.1080/19475705.2024.2384607
Chwikhi W, Abdelkrim B, Atoui M, Bouajila A, Antunes I, Dhaouadi L, Mahmoudi S. 2025. Integrated AHP-GIS modeling for soil erosion risk assessment in arid regions: a case study of Gabès, Tunisia. Earth Syst Environ. 735. https://doi.org/10.1007/s41748-025-00735-7
Daliakopoulos I, Tsanis I, Koutroulis A, Kourgialas N, Varouchakis A, Karatzas G, Ritsema C. 2016. The threat of soil salinity: a European scale review. Sci Total Environ. 573:727–739. https://doi.org/10.1016/j.scitotenv.2016.08.177
DeSA UN. 2013. World population prospects: the 2012 revision. Population division of the department of economic and social affairs of the United Nations Secretariat. 18. New York. p 620–626.
Di Salvo C, Ciotoli G, Mancini M, Nisio S, Stigliano F. 2024. Analysis of geological multi-hazards in an Urban District. Geosciences (Switzerland). 14(2):27. https://doi.org/10.3390/geosciences14020027
Dieno W, Pathan S. 2025. Flood susceptibility mapping and 3d flood simulation in the jia bharali river basin, sonitpur district, india, using the analytical hierarchy process (AHP). Remote Sens Earth Syst Sci. 8(3):881–911. https://doi.org/10.1007/s41976-025-00226-3
El baida M, Boushaba F, Chourak M, Hosni M, Sabar H, Zahaf T. 2024. Flood risk decomposed: optimized machine learning hazard mapping and multi-criteria vulnerability analysis in the city of Zaio, Morocco. JAfES. 220:105431. https://doi.org/10.1016/j.jafrearsci.2024.105431
Elhag M. 2016. Evaluation of different soil salinity mapping using remote sensing techniques in arid ecosystems, Saudi Arabia. J Sens. 2016:1–8. https://doi.org/10.1155/2016/7596175
Elomiya A, Křupka J, Jovčić S, Simic V, Švadlenka L, Pamucar D. 2024. A hybrid suitability mapping model integrating GIS, machine learning, and multi-criteria decision analytics for optimizing service quality of electric vehicle charging stations. Sustain Cities Soc. 106:105397. https://doi.org/10.1016/j.scs.2024.105397
Elsamani Y, Almuslem A, Tokhi M. 2001. Geology and geotectonic classification of pan-african gold mineralizations in the red sea hills, sudan. Int Geol Rev. 43(12):1117–1128. https://doi.org/10.1080/00206810109465064
Elsayed Zeinelabdein K, Mohamed E, Elsheikh A. 2021. Applications of remote sensing and GIS in geological mapping, mineral prospecting and groundwater investigations in the Arabian-Nubian Shield: cases from the Red Sea Hills of NE Sudan. In: Hamimi Z, Fowler A-R, Liégeois J-P, Collins A, Abdelsalam MG, Abd EI-Wahed M, editors. The Geology of the Arabian-Nubian Shield. Springer International Publishing: Cham. p 659–686. https://doi.org/10.1007/978-3-030-72995-0_25.
Erol A. 1989. Engineering geological considerations in a salt dome region surrounded by sabkha sediments, Saudi Arabia. Eng Geol. 26(3):215–232. https://doi.org/10.1016/0013-7952(89)90010-0
Ferreira Z, Almeida B, Costa A, do Couto Fernandes M, Cabral P. 2025. Insights into landslide susceptibility: a comparative evaluation of multi-criteria analysis and machine learning techniques. Geomat, Nat Hazards and Risk. 16(1), https://doi.org/10.1080/19475705.2025.2471019
Loughland RA, Qasem AM, Burwell B, Prihartat PK. 2018. Coastal Sabkha (Salt Flats) of the Southern and Western Arabian Gulf. In: Finlayson C, Milton, G, Prentice R, Davidson N, editors. The Wetland Book. Springer: Dordrecht. https://doi.org/10.1007/978-94-007-4001-3_185
Gau H, Hsieh C, Liu C. 2006. Application of grey correlation method to evaluate potential groundwater recharge sites. Stoch Environ Res Risk Assess. 20(6):407–421. https://doi.org/10.1007/s00477-006-0034-9
Ghazali M, Wikantika K, Harto A, Kondoh A. 2020. Generating soil salinity, soil moisture, soil pH from satellite imagery and its analysis. Info Process Agric. 7(2):294–306. https://doi.org/10.1016/j.inpa.2019.08.003
Gholizadeh A, Mokhtari M, Naimi N, Shiravand B, Ehrampoush M, Miri M, Ebrahimi A. 2017. Assessment of corrosion and scaling potential in groundwater resources; a case study of Yazd-Ardakan Plain, Iran. Groundw Sustain Dev. 5:59–65. https://doi.org/10.1016/j.gsd.2017.04.002
Godes C, Lim O, Rodrigazo S, Kim Y, Kim Y, Lee S, Yeon J. 2025. Advancing geohazard risk assessment – a digital tool for steep slope management. Prog Disaster Sci. 26:100418. https://doi.org/10.1016/j.pdisas.2025.100418
Gogu R, Dassargues A. 2000. Sensitivity analysis for the EPIK method of vulnerability assessment in a small karstic aquifer, southern Belgium. Hydrogeol J. 8(3):0337. https://doi.org/10.1007/s100400050019
Gohil M, Mehta D, Shaikh M. 2024. An integration of geospatial and fuzzy-logic techniques for multi-hazard mapping. Res Eng. 21:101758. https://doi.org/10.1016/j.rineng.2024.101758
Griffiths J, Fookes P, Goudie A, Stokes M, Party EGW. 2012. Chapter 3 processes and landforms in deserts. Geol Soc Lond Eng Geol Spec Publ. 25(1):33–95. https://doi.org/10.1144/EGSP25.03. .
Ha H, Luu C, Bui Q, Nguyen V, Vu N, Kervyn M. 2025. Landslide risk assessment using an integrated framework of machine learning algorithms and multi-criteria decision analysis. Nat Hazards. 121:19723–19759. https://doi.org/10.1007/s11069-025-07583-8
Hamid O. 2022. Hydro-environmental impact of Khor Arbaat Dam, Eastern Sudan. Int J Water Resour Environ Eng. 14(1):1–11. https://doi.org/10.5897/IJWREE2022.1027
Hartemink A, Krasilnikov P, Bockheim J. 2013. Soil maps of the world. Geoderma. 207:256–267. https://doi.org/10.1016/j.geoderma.2013.05.003
Hawash E, El-Hassanin A, Amer W, El-Nahry A, Effat H. 2021. Change detection and urban expansion of Port Sudan, Red Sea, using remote sensing and GIS. Environ Monit Assess. 193(11):723. https://doi.org/10.1007/s10661-021-09486-0

He J, Zhao W, Li A, Wen F, Yu D. 2019. The impact of the terrain effect on land surface temperature variation based on Landsat-8 observations in mountainous areas. Int J Remote Sens. 40(5–6):1808–1827. https://doi.org/10.1080/01431161.2018.1466082

Hird R, Di Matteo N, Gulerce U, Sunderlal Babu V, Rafiq A. 2019. Geohazards of Saudi Arabia. J Maps. 15(2):626–634. https://doi.org/10.1080/17445647.2019.1642245

Huang P, Wu X, Ma C, Zhou A. 2023. Geo-environment vulnerability assessment of multiple geohazards using VWT-AHP: a case study of the Pearl River Delta, China. Remote Sens (Basel). 15(20):5007. https://doi.org/10.3390/rs15205007

Kainthura P, Sharma N. 2022. Hybrid machine learning approach for landslide prediction, Uttarakhand, India. Sci Rep. 12(1):20101. https://doi.org/10.1038/s41598-022-22814-9

Kenea NH, Ebinger CJ, Rex DC. 2001. Late Oligocene volcanism and extension in the southern Red Sea Hills, Sudan. J Geol Soc. 158:285–294. https://doi.org/10.1144/jgs.158.2.285.

Köppen W. 1900. Versuch einer Klassifikation der Klimate, vorzugsweise nach ihren Beziehungen zur Pflanzenwelt. Geogr Z. 6(11):593–611. http://www.jstor.org/stable/27803924.

Kottek M, Grieser J, Beck C, Rudolf B, Rubel F. 2006. World map of the Köppen-Geiger climate classification updated. Meteorol Z. 15(3):259–263. https://doi.org/10.1127/0941-2948/2006/0130

Laurila T, Hannington M, Leybourne M, Petersen S, Devey C, Garbe-Schönberg D. 2015. New insights into the mineralogy of the Atlantis II Deep metalliferous sediments, Red Sea. GGG. 16(12):4449–4478. https://doi.org/10.1002/2015GC006010

Lavanya M, Muthukumar M. 2024. AHP and geospatial technologies for identifying groundwater exploration target regions in Dindigul, southern India. Geo Geo. 3(4):100315. https://doi.org/10.1016/j.geogeo.2024.100315

Lee EM, Griffiths JS. 2024. What is a geohazard? Q J Eng Geol Hydrogeol. 57(4):qjegh2024-034. https://doi.org/10.1144/qjegh2024-034

Lerdsuwankij T, Cavalleri C, Wanwises J, 2024. De-risking shallow gas Hazards: case studies on the effectiveness of an innovative pulsed neutron logging tool; Kuala Lumpur, Malaysia. The Offshore Technology Conference Asia. https://doi.org/10.4043/34790-MS

Liu S, Wang L, Zhang W, He Y, Pijush S. 2023. A comprehensive review of machine learning-based methods in landslide susceptibility mapping. Geol J. 58(6):2283–2301. https://doi.org/10.1002/gj.4666

Ma Z, Mei G. 2021. Deep learning for geological hazards analysis: data, models, applications, and opportunities. Earth Sci Rev. 223:103858. https://doi.org/10.1016/j.earscirev.2021.103858

Malczewski J, Rinner C. 2015. GIS-MCDA for Group Decision Making. In: Multicriteria Decis Anal Geogr Inf Sci. Springer. p 223–247. https://doi.org/10.1007/978-3-540-74757-4_8.

Maleki S, Pouyan S, Khoshoui M, Tiefenbacher J, Pourghasemi H. 2024. Detecting soil salinization, sodicity, and alkalization hazards within cultivated lands using digital soil mapping approaches. In: Advanced Tools for Studying Soil Erosion Processes. Elsevier. p 435–460. https://doi.org/10.1016/B978-0-443-22262-7.00019-9

Mao Y, Zhu L, Chen J, Nanehkaran Y. 2024. Adaptive modeling of landslide susceptibility using analytical hierarchy process and multi-objective decision optimization. AdSpR. 75(6):4536–4551. https://doi.org/10.1016/j.asr.2024.12.061

Mason P, Rosenbaum M. 2002. Geohazard mapping for predicting landslides: an example from the Langhe Hills in Piemonte, NW Italy. Q J Eng Geol Hydrogeol. 35(4):317–326. https://doi.org/10.1144/1470-9236/00047

Nagamani K, Mishra A, Meer M, Das J. 2024. Understanding flash flooding in the Himalayan region: a case study. Sci Rep. 14(1):7060. https://doi.org/10.1038/s41598-024-53535-w

Niclòs R, Puchades J, Coll C, Barberà M, Pérez-Planells L, Valiente J, Sánchez J. 2021. Evaluation of Landsat-8 TIRS data recalibrations and land surface temperature split-window algorithms over a homogeneous crop area with different phenological land covers. JPRS. 174:237–253. https://doi.org/10.1016/j.isprsjprs.2021.02.005

Obiegbu O. 2021. Geohazard characterization using remote sensing to model flash floods of the southeast Sinai, Egypt. Interpretation. 9(3):T821–T831. https://doi.org/10.1190/INT-2020-0115.1

Panchal S, Shrivastava K. 2022. Landslide hazard assessment using analytic hierarchy process (AHP): a case study of National Highway 5 in India. Ain Shams Eng J. 13(3):101626. https://doi.org/10.1016/j.asej.2021.10.021

Patel D, Thakur T, Thakur A, Karuppannan S, Swamy S, Pant R. 2024. Groundwater potential zone mapping using AHP and geospatial techniques in the upper Narmada basin, central India. DiSus. 5(1):355. https://doi.org/10.1007/s43621-024-00560-4

Lokesh P, Madhesh C, Mathew A, Shekar PR. 2025. Machine learning and deep learning-based landslide susceptibility mapping using geospatial techniques in Wayanad, Kerala state, India. HydroResearch. 8:113–126. https://doi.org/10.1016/j.hydres.2024.10.001

Rajendran S, Al-Kuwari H, Sadooni F, Nasir S, Govil H. 2021. Remote sensing of inland Sabkha and a study of the salinity and temporal stability for sustainable development: a case study from the West coast of Qatar. Sci Total Environ. 782:146932. https://doi.org/10.1016/j.scitotenv.2021.146932

Rashwan M, Mohamed L, Hassan A, Youssef M, Sabra M, Mohamed A. 2024. Landslide susceptibility assessment along the Red Sea Coast in Egypt, based on multi-criteria spatial analysis and GIS techniques. Sci Afr. 23:e02116. https://doi.org/10.1016/j.sciaf.2024.e02116

Rengasamy P, de Lacerda C, Gheyi H. 2022. Salinity, sodicity and alkalinity. In: Subsoil constraints for crop production. Springer: place unknown. p 83–107. https://doi.org/10.1007/978-3-031-00317-2_4

Sulieman HM, Andersen GL, Mohamed T. 2024. Social and Spatial Flood Risk Analysis for Decision Making: Cases from Two Flood Prone Areas in Eastern Sudan. Bergen: Chr. Michelsen Institute. https://www.cmi.no/publications/9426-social-and-spatial-flood-risk-analysis-for-decision-making

Saaty R. 1987. The analytic hierarchy process—what it is and how it is used. Math Modelling. 9(3–5):161–176. https://doi.org/10.1016/0270-0255(87)90473-8

Sahab S, Suhani I, Srivastava V, Chauhan P, Singh R, Prasad V. 2021. Potential risk assessment of soil salinity to agroecosystem sustainability: current status and management strategies. Sci Total Environ. 764:144164. https://doi.org/10.1016/j.scitotenv.2020.144164

Sandoval V, Voss M, Flörchinger V, Lorenz S, Jafari P. 2023. Integrated disaster risk management (IDRM): elements to advance its study and assessment. Disaster Risk Sci. 14(3):343–356. https://doi.org/10.1007/s13753-023-00490-1

Saptutyningsih E, Dewanti D. 2023. Measuring the economic impact of landslide hazard: hedonic price approach. IOP Conf Ser Earth Environ Sci. 1180(1):012048. https://doi.org/10.1088/1755-1315/1180/1/012048

Semnani S, Han Y, Bonfils C, White J. 2025. Assessing the impact of climate change on rainfall-triggered landslides: a case study in California. Landslides. 22:1707–1724. https://doi.org/10.1007/s10346-024-02428-0

Shebl A, Abdelaziz M, Ghazala H, Araffa S, Abdellatif M, Csámer A. 2022. Multi-criteria ground water potentiality mapping utilizing remote sensing and geophysical data: a case study within Sinai Peninsula, Egypt. Egypt J Remote Sens Space Sci. 25(3):765–778. https://doi.org/10.1016/j.ejrs.2022.07.002

Shou K, Lin J. 2020. Evaluation of the extreme rainfall predictions and their impact on landslide susceptibility in a sub-catchment scale. Eng Geol. 265:105434. https://doi.org/10.1016/j.enggeo.2019.105434

Shu B, Liu Y, Wang C, Zhang H, Amani-Beni M, Zhang R. 2024. Geological hazard risk assessment and rural settlement site selection using GIS and random forest algorithm. Ecol Indic. 166:112554. https://doi.org/10.1016/j.ecolind.2024.112554

Stern R, Kroner A, Manton W, Reischmann T, Mansour M, Hussein I. 1989. Geochronology of the late Precambrian Hamisana shear zone, Red Sea Hills, Sudan and Egypt. J Geol Soc (London). 146(6):1017–1029. https://doi.org/10.1144/gsjgs.146.6.1017

Tavakoli M, Motlagh Z, Dąbrowska D, Youssef Y, Đurin B, Saqr A. 2025. Harnessing AHP and Fuzzy Scenarios for Resilient Flood Management in Arid Environments: Challenges and Pathways Toward Sustainability. Water (Basel). 17(9):1276. https://doi.org/10.3390/w17091276

Tesfa C. 2025. Geohazard mapping and mitigations along the road corridor Gasera–Indeto, Southeast Ethiopia. Environ Sustain Indic. 25:100570. https://doi.org/10.1016/j.indic.2024.100570

Ullah N, Tariq A, Qasim S, Panezai S, Uddin M, Abdullah-Al-Wadud M, Ullah S. 2024. Geospatial analysis and AHP for flood risk mapping in Quetta, Pakistan: a tool for disaster management and mitigation. Appl Water Sci. 14(11):236. https://doi.org/10.1007/s13201-024-02293-1

Vanhellemont Q. 2020. Combined land surface emissivity and temperature estimation from Landsat 8 OLI and TIRS. JPRS. 166:390–402. https://doi.org/10.1016/j.isprsjprs.2020.06.007

Vaziri V, Khademi Hamidi J, Sayadi A. 2018. An integrated GIS-based approach for geohazards risk assessment in coal mines. Environ Earth Sci. 77(1):29. https://doi.org/10.1007/s12665-017-7198-0

Wahba D, Omran A, Adly A, Gad A, Arman H, El-Bagoury H. 2024. Optimizing site selection for construction: integrating gis modeling, geophysical, geotechnical, and geomorphological data using the analytic hierarchy process. ISPRS Int J Geoinf. 14(1):3. https://doi.org/10.3390/ijgi14010003

Whiteman A. 1970. Comments on the classification of the basement complex of the red sea hills. place unknown.

Williams M. 2019. The Red Sea Hills. In: Williams M, editor. The Nile Basin: Quaternary Geology, Geomorphology and Prehistoric Environments [Internet]. Cambridge: Cambridge University Press; p 257–266. https://doi.org/10.1017/9781316831885.019.

Xu X, Cui P, Zhang X. 2024. Critical environmental factors affecting mountain geohazards in a warming climate in Southwest China. Adv Clim Change Res. 15(4):695–707. https://doi.org/10.1016/j.accre.2024.07.006

Youssef El Sayed AA. 1991. A Note on the Geomorphology of the Coastal Plain between Al Hudaydah and Al Salif Peninsula, Red Sea Coast, Yemen Arab Republic. Geogr J. 15(1):71–73. https://doi.org/10.2307/635146

Yaghoubi E, Yaghoubi E, Khamees A, Vakili A. 2024. A systematic review and meta-analysis of artificial neural network, machine learning, deep learning, and ensemble learning approaches in field of geotechnical engineering. Neural Comput Appl. 36(21):12655–12699. https://doi.org/10.1007/s00521-024-09893-7

Zhang C, Xu B, Chu C, Ye P, Zhang X, Zhou K, Liu W. 2025. Landslide knowledge representation based on hypergraph theory. Trans GIS. 29(1):e13276. https://doi.org/10.1111/tgis.13276

Zhou L, Liu L. 2024. Enhancing dynamic flood risk assessment and zoning using a coupled hydrological-hydrodynamic model and spatiotemporal information weighting method. J Environ Manage. 366:121831. https://doi.org/10.1016/j.jenvman.2024.121831

Zou F, Che E, Long M. 2023. Quantitative assessment of geological hazard risk with different hazard indexes in mountainous areas. J Clean Prod. 413:137467. https://doi.org/10.1016/j.jclepro.2023.13746